Check for updates

Received: 14 February 2023 | Revised: 19 May 2023 | Accepted: 1 June 2023

DOI: 10.1002/dep2.240

The Depositional Record
A journal of the International Association of Sedimentologists
Open Access
IAS
WILEY

ORIGINAL RESEARCH ARTICLE

Interactions between distal epiclastic and bio-chemogenic sedimentation at the foothills of a mafic alkaline volcano: The case of the Oligocene Doupovské Hory Volcanic Complex (Czech Republic)

Vladislav Rapprich[1] | **Pavel Čáp**[1] | **Yulia V. Erban Kochergina**[1] | **Eva Kadlecová**[1] | **Zsolt Benkó**[2] | **Jakub Sakala**[3] | **Zuzana Rodovská**[1] | **Jan Matějů**[4] | **Daniel A. Petrash**[1]

[1]Czech Geological Survey, Prague, Czech Republic

[2]Institute for Nuclear Research, Debrecen, Hungary

[3]Institute of Geology and Palaeontology, Faculty of Science, Charles University, Prague, Czech Republic

[4]The Karlovy Vary Museum, Karlovy Vary, Czech Republic

Correspondence
Vladislav Rapprich, Czech Geological Survey, Klárov 3, 118 21 Prague, Czech Republic.
Email: vladislav.rapprich@geology.cz

Funding information
Česká geologická služba, Grant/Award Number: 311150

Abstract

Late Oligocene (*ca* 25 Ma) volcano-sedimentary successions exposed on the western periphery of the Doupovské Hory Volcanic Complex reveal a complex sedimentation history influenced in various ways by decay of the alkali basalt volcanic edifice. Weathering of the volcanic rocks supplied abundant reactants that promoted carbonate precipitation in the peripheral palaeolakes—as evidenced by strongly non-radiogenic $^{87}Sr/^{86}Sr$ values (0.7038–0.7041). On the other hand, the sediments of the initial shallow lake became deformed by the bulldozing effect of a debris avalanche. The debris flow and avalanche deposits filled up the original depression, modified the basin morphology and shifted the peripheral lacustrine setting further away from the volcano. At this stage, surface water influx from the surrounding granites conferred a more radiogenic character ($^{87}Sr/^{86}Sr$ values 0.7046–0.7049) to the calcrete deposits. Fossil assemblages as well as limestone textures suggest significant seasonal water-level fluctuations, possibly reflecting the alternating rainy and dry-seasons of a prevalently humid Central-European Late Oligocene climate. The seasonal drying out of the ponds resulted in significant ^{18}O enrichments. Although the *ca* 0‰ $\delta^{13}C$ values might suggest mixing of atmospheric and volcanic CO_2 during carbonate precipitation, no active volcanic conduits of relevant age are known in the close vicinity. The lower $\delta^{13}C$ values are likely a result of mantle degassing through rift faults, a phenomenon observed in the magmatically extinct Ohře Rift until present. This paper demonstrates that limestones derived from weathered alkaline basalts are characterised by highly non-radiogenic Sr isotopic ratios ($^{87}Sr/^{86}Sr$ *ca* 0.704), suggesting a magmatic origin for the Ca within these carbonates. Contrary to the notion of carbonatites being present when highly non-radiogenic Sr isotopes are found, these results show that Sr isotopes

This is an open access article under the terms of the Creative Commons Attribution License, which permits use, distribution and reproduction in any medium, provided the original work is properly cited.
© 2023 The Authors. *The Depositional Record* published by John Wiley & Sons Ltd on behalf of International Association of Sedimentologists.

in carbonates formed in alkali basalt-sourced environments only reveal the source of the Sr (and Ca) ions, not necessarily the presence of carbonatite.

KEYWORDS

Doupovské Hory Volcanic Complex, freshwater limestone, gastropod palaeoecology, kinetic deformations, lahar, Sr-C-O-isotope systematics

1 | INTRODUCTION

Volcanoes are frequently associated with sedimentary basins, which they supply with clastic material (Di Capua & Groppelli, 2018; Hroch et al., 2012; Kataoka et al., 2009; Manville et al., 2009; Martí et al., 2018; Novo et al., 2018; Ollier et al., 1998; White & Riggs, 2009). Desublimation of volcanic gases may deposit significant amounts of chemical deposits, such as travertine (Garavelli et al., 1997). From another point of view, the sedimentary basement beneath a volcanic edifice may cause instability, sliding or even triggering catastrophic sector collapses (Francis et al., 1985; Murray et al., 2018; Tibaldi & Lagmay, 2006; Van Wyk de Vries et al., 2001). Once the volcano edifice fails producing a debris flow or avalanche, these sliding high-energy masses may deform the plastic rocks located within the foothills of the volcano, as observed in numerous Quaternary volcanoes (Dufresne et al., 2010; Kühn et al., 2021; Roberti et al., 2017; Watt et al., 2012).

In the western foothills of the Oligocene to Early Miocene Doupovské Hory alkaline shield volcano, limited outcrops of limestone are found in association with volcanic agglomerates. The scarcity of comparable volcano-sedimentary systems in the literature, both for recent and ancient complexes, provided the motivation to deepen the understanding of this depositional association. Although the limited number of exposures and the localised nature of this study prevent a comprehensive reconstruction of the volcano's entire depositional history, involving multiple stages of edifice growth and decay, this research does shed light on the complex interplay between volcanic processes, carbonate sedimentation and palaeoenvironmental conditions.

This paper contributes to a better understanding of the interactions between epiclastic (volcanogenic) and biochemogenic sedimentation in alkaline volcanic systems, as well as the broader implications for interpreting Sr isotopes in alkaline basalt weathering-redeposition mechanisms. To achieve these objectives, a multidisciplinary study was conducted incorporating volcanology, sedimentary petrology, palaeobiology, geochemistry, geochronology and C-O-Sr isotopic systematics, including leaching experiments.

2 | GEOLOGICAL SETTING

The Doupovské Hory Volcanic Complex (DHVC) is one of the major remnants of Cenozoic alkaline magmatism in the Bohemian Massif in Central Europe (Figure 1A). The abundance of volcanic rocks in the Bohemian Massif follows the Variscan suture between the Saxothuringian and Teplá-Barrandian domains (Mlčoch & Konopásek, 2010). Two volcanic complexes and several volcanic fields erupted along this suture (Ackerman et al., 2015; Rapprich & Holub, 2008), but also numerous volcanic fields erupted further away from this zone (Rapprich et al., 2007; Figure 1B). Apart from a short period of magmatism around the K-Pg boundary, Cenozoic activity in the Bohemian Massif lasted from the Late Eocene until the Pleistocene (Ulrych et al., 2011). Volcanic activity in the DHVC itself started in the lowermost Oligocene (Fejfar & Kaiser, 2005), culminated in the early Oligocene (Holub et al., 2010) and lasted until the early Miocene (Sakala et al., 2010). Subsequently, the Miocene Ohře (Eger) Rift, representing the easternmost branch of the European Cenozoic Rift System (Dèzes et al., 2004), developed along the same Variscan suture zone (Rajchl et al., 2009). The entire volcanic edifice developed as a multiphase shield volcano dominated by lavas of alkaline basaltic composition. Subsidence of the Ohře Rift then contributed to the preservation of thick superficial volcanic sequences by limiting erosion. The preserved sequences are dominated by lava flows (Rapprich & Holub, 2008), associated with numerous deposits of lahars and debris avalanches suggesting several stages where the volcanic edifice decayed and was then rebuild (Rapprich & Dostalík, 2015; Sakala et al., 2010). Concurrently with volcanic activity, agglomerates (or debrites: lahars and debris avalanches deposits) sourced from slope-failure processes formed fans at the foothills of the volcanic complex. Here the focus is on the margin of one of such agglomerate fan in the western DHVC foothills (Figure 1C). It recorded interactions between volcanic and lacustrine palaeoenvironments.

On the western margin of the DHVC (Figure 1C), limestone occurrences associated with volcaniclastic deposits were first reported in the late 18th century. Mining of 'hard' limestone ('quarry' site in Figure 1C) near the

20554877, 2023, 4, Downloaded from https://onlinelibrary.wiley.com/doi/10.1002/dep2.240 by Cochrane Hungary, Wiley Online Library on [05/12/2023]. See the Terms and Conditions (https://onlinelibrary.wiley.com/terms-and-conditions) on Wiley Online Library for rules of use; OA articles are governed by the applicable Creative Commons License

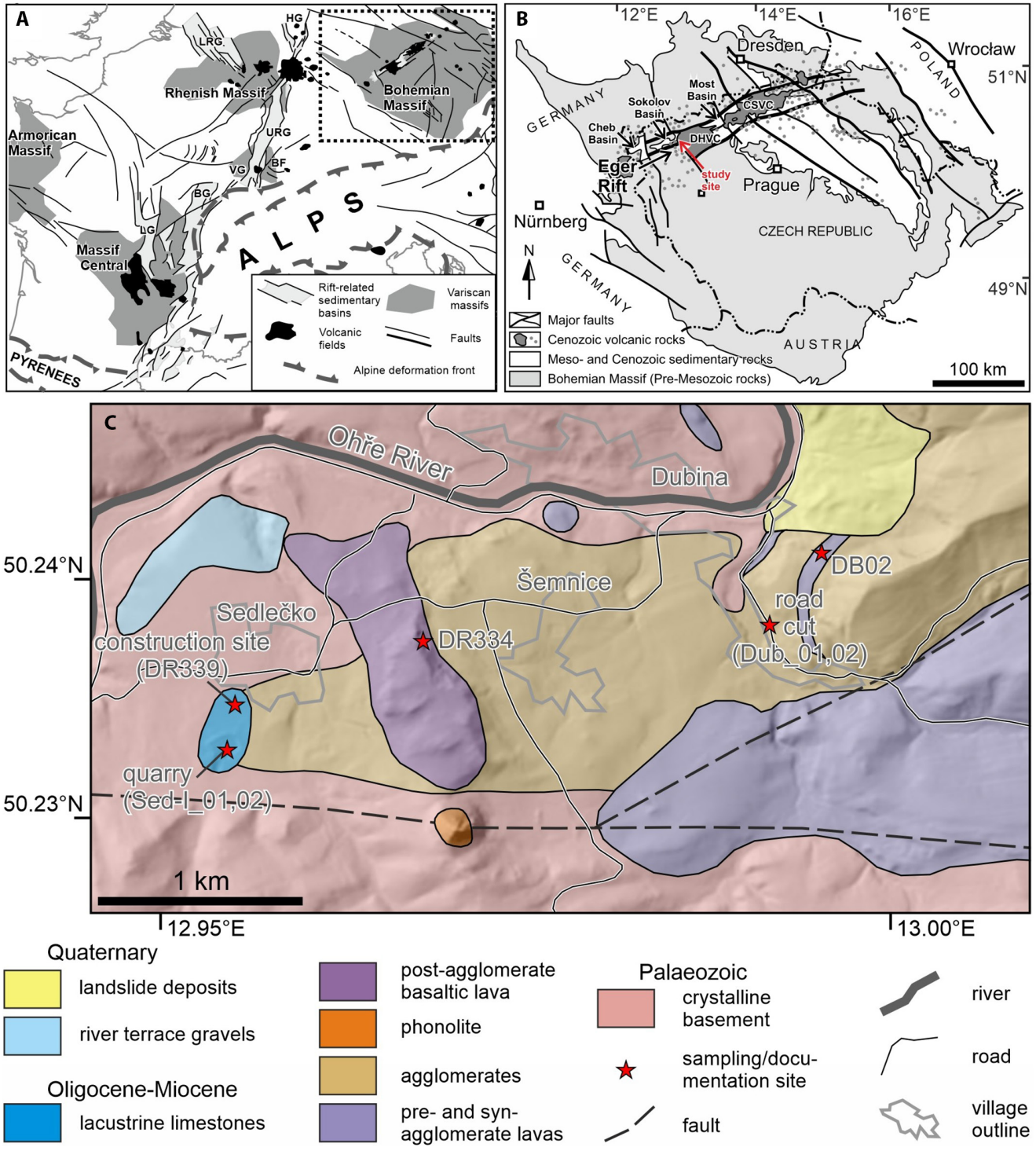

FIGURE 1 Location map of the study area: (A) within the European Cenozoic Rift System (adapted after Dèzes et al., 2004); (B) among the Cenozoic alkaline volcanic systems of the Bohemian Massif (adopted from Holub et al., 2010). (C) Geological sketch map of the study area.

village of Sedlečko was first mentioned by Schaller (1785). Glückselig (1842) appended that an outcrop of limestone in basaltic tuffs could be also found near Dubina ('road-cut' site in Figure 1C). The limestones from both localities were described as fine-grained, yellowish, and containing abundant leaf imprints. Glückselig (1842) also mentioned the limestone from Sedlečko. Exploitation in the quarry was complemented by short shafts and two adits drained by a steam pump, this ended in 1890 when the deposit was exhausted (Zerlik et al., 1974). The Sedlečko limestone quarry attracted the attention of palaeontologists since the mid-19th century. Reuss and von Meyer (1849)

20554877, 2023, 4, Downloaded from https://onlinelibrary.wiley.com/doi/10.1002/dep2.240 by Cochrane Hungary, Wiley Online Library on [05/12/2023]. See the Terms and Conditions (https://onlinelibrary.wiley.com/terms-and-conditions) on Wiley Online Library for rules of use; OA articles are governed by the applicable Creative Commons License

and Reuss (1854, 1863) were impressed by the richness of the imprints of dicotyledonous leaves in the limestone. However, the same authors noted a lack of fossil fauna.

3 | METHODS

3.1 | Field documentation, sample preparation

The entire DHVC is encircled by several agglomerate (lahar) fans (Rapprich & Dostalík, 2015; Sakala et al., 2010) developed during multi-phase growth and decay of the volcanic complex. The agglomerate fan in the western foothills studied here (Figure 1C) represents proximal facies exposed during reconstruction of the road-cut near Dubina, whereas the distal facies, where the lahar transitions into a lacustrine environment, are exposed in an abandoned limestone quarry near Sedlečko. An additional limestone occurrence near the Sedlečko quarry was temporarily exposed by excavation during construction of a house (Figure 1C). All three exposures are documented in detail here, with samples collected for further analytical work.

Thin sections from representative rock samples were prepared in the laboratories of the Czech Geological Survey (CGS), and studied under a petrographic microscope (Nikon Eclipse 80i). Fossils were mechanically separated before final cleaning with a vibro-tool. Carbonate fossils enclosed in carbonate rocks precluded the application of acid in fossil separation, except for marginal application of 8% acetic acid. Zoopalaeontological material described in this study is archived in the palaeontological collection of the CGS, while the palaeobotanical samples are stored in the repository of the Karlovy Vary Museum. Five representative samples of limestone were collected for geochemical and isotopic analyses conducted in the laboratories of the CGS in Prague. Two samples of basaltic lavas, one interbedding the debrite sequence and the other overlaying the debrites (Figure 1C), were collected for K-Ar geochronology.

3.2 | Bulk-rock chemistry

Whole-rock major-element concentrations (including volatiles: moisture, bound water, CO_2, S and F) were determined in the CGS laboratories employing conventional wet chemistry involving titration, flame photometry and atomic adsorption spectrometry (Dempírová et al., 2010). The samples were first dissolved using $HF+HNO_3+H_2SO_4$ at 220°C (determination of SiO_2), and subsequently in a $HCl+H_2SO_4$ mixture (remaining oxides). Trace-element contents were determined using an Agilent Technologies 7900 series ICP-MS. Prior to rare earth element (REE) determination, the samples were fused with $LiBO_2$ (after removal of organic compounds) and dissolved in dilute HCl. Additional trace elements (Ba, Cr, Ga, Hf, Nb, Ni, Pb, Rb, Sc, Sr, Ta, Th, U, V, Y, Zr) were determined after acid digestion with HF (total dissolution of sample with HF, treatment with $HClO_4$ and H_3BO_3 mixture and redissolution with HNO_3 after drying). Data handling and plotting were performed using GCDkit software (Janoušek et al., 2006).

3.3 | Stable C-O isotopes

Stable C-O isotopic compositions were evaluated, after removal of organic carbon with H_2O_2, by implementing the method described by McCrea (1950). Samples of carbonate were decomposed by 100% H_3PO_4 under vacuum at 25°C. The carbon and oxygen isotopic composition of the evolved CO_2 gas was measured using a dual inlet DeltaV Advantage IRMS (Delta V Isotope Ratio Mass Spectrometer), in the CGS laboratories. The results are reported in conventional δ ($\delta = R_{sample}/R_{standard} - 1$, where R is the mole ratio of $^{13}C/^{12}C$ or $^{18}O/^{16}O$) notation relative to V-SMOW (Vienna Standard Mean Ocean Water standard) for oxygen and V-PDB (Vienna Pee Dee Belemnite standard) for carbon. The analytical error was ±0.1‰ for both $\delta^{13}C$ and $\delta^{18}O$ values. The accuracy of the measurement was checked by analyses of the international standard (IAEA) NBS 18 ($\delta^{13}C = -5.014$‰, $\delta^{18}O = -23.2$‰) and two in-house standards: Carrara marble ($\delta^{13}C = 2.29$‰, $\delta^{18}O = -1.32$‰) and CS 2 ($\delta^{13}C = 2.93$‰, $\delta^{18}O = -3.86$‰). The long-term reproducibility for all standards is better than 0.05‰ for $\delta^{13}C$ and 0.1 for $\delta^{18}O$.

3.4 | Radiogenic Sr isotopes

Five limestone samples were analysed for Sr isotopes. In order to better understand the carbonate source, four samples of recent hot-spring travertines from Karlovy Vary (5 km to the west of the studied area), as well as leachates and residuals of four representative basaltic lavas and a lahar deposit were prepared to complement the dataset.

Chemical separations for Sr isotope analyses were performed in a class ISO 7 ultra-clean laboratory at CGS. Doubly distilled acids were used for the Sr separation procedure and 18.2 MΩ·cm Milli-Q water was used throughout. Additional details of the sample preparation procedure are described in Erban Kochergina et al. (2021, 2022). For each sample, about 100 mg of powdered carbonate rock was dissolved in 6 M HCl in Savillex® vials, water samples were evaporated to dryness and then dissolved in a H_2O_2 and HNO_3 mixture (Erban Kochergina et al., 2021).

20554877, 2023, 4, Downloaded from https://onlinelibrary.wiley.com/doi/10.1002/dep2.240 by Cochrane Hungary, Wiley Online Library on [05/12/2023]. See the Terms and Conditions (https://onlinelibrary.wiley.com/terms-and-conditions) on Wiley Online Library for rules of use; OA articles are governed by the applicable Creative Commons License

About 200 mg of each of the four samples of basaltic rocks representing the prevailing lavas of the DHVC (Rapprich & Holub, 2008) and one sample of lahar deposit from Sedlečko quarry were leached in ascorbic acid (for details see Kochergina et al., 2017; Nádaskay et al., 2019). The leachates were evaporated to dryness, dissolved in a H_2O_2–HNO_3 mixture, and re-dissolved in 2 M HNO_3. Residual phases were removed by centrifugation. Then, the residuum was dissolved as a silicate rock sample in a HF–HNO_3 mixture (3:1, v/v).

The Sr.spec resin (Triskem Intl.) was employed for final purification of the Sr fraction (Erban Kochergina et al., 2022). Strontium isotope analyses were performed on a Triton Plus TIMS, using a single Ta filament assembly. The external reproducibility of the obtained data is given by repeated analyses of the SRM 987 standard $^{87}Sr/^{86}Sr = 0.710255 \pm 08$ (2SM, $n = 1$). The carbonate reference material EN-1 yielded a $^{87}Sr/^{86}Sr$ value of 0.709194 ± 09 (2SM, $n = 1$), JB-3 basalt $^{87}Sr/^{86}Sr = 0.703416 \pm 09$ (2SM, $n = 1$). The decay constants of ^{87}Rb applied to age-correct the isotopic Sr ratios are from Villa et al. (2015, 2020).

3.5 | Geochronology

Two samples of basaltic lavas were collected. These include lava of fine-grained aphanitic limburgite embedded within the agglomerate (lahar and debris avalanche deposits) sequence (DB02) and alkaline basalt lava covering the entire studied sequence (DR334). Whole-rock samples were analysed by the unspiked K-Ar method, following the procedure laid out by Matsumo and Kobayashi (1995) in the Geochronology Laboratory of the Institute for Nuclear Research, Debrecen, Hungary. Potassium content was measured on 50 mg sample aliquots, after dissolution by HF and HNO_3, with a Sherwood-400-type flame spectra-photometer with accuracy better than ±1%. Separated mineral sample splits were then subjected to heating at 100°C for 24 h under vacuum, to remove atmospheric Ar contamination that was adsorbed on the surface of the mineral particles during sample preparation. Argon was extracted from the minerals by fusing the samples via high-frequency induction heating at 1,300°C. The released gases were cleaned in two steps in a low-blank vacuum system by cold St-707 and hot Ti-getters. The isotopic composition of the Ar was measured using an Argus VI© multi-collector noble gas mass spectrometer and corrected for atmospheric $^{40}Ar/^{36}Ar$ ratios. The accuracy and reproducibility of isotope ratio measurements were periodically controlled with the HDB-1 (Hess & Lippolt, 1994) and MDO-G (Gillot et al., 1992) international standards. Decay constants recommended by Steiger and Jäger (1977) were used for age calculations, with an overall error of ±1%. Error of the samples was calculated using the equation of Quidelleur et al. (2001).

4 | RESULTS

4.1 | Lithofacies distribution and petrography

4.1.1 | Dubina road-cut

In the studied transition of agglomerate fan into marshy plains at the volcano foothills, the proximal facies of the investigated sedimentary system consists of volcanoclastic and sedimentary rocks displaying irregular boundaries (Figure 2A), with (sub)horizontal bedding seen only locally (Figure 2B). The bio-chemogenic sedimentary rocks (limestone, diatomite) in the Dubina section are present mostly in the form of deformed fragments within the debrite deposits (rip-up clasts; Tost et al., 2014). The laminated sediments adjacent to the agglomerate (debrite) accumulation are intensively folded (Figure 2C). The original horizontal position was revealed only at the base of the section, underlying the debrites.

In total, six lithofacies are exposed in the Dubina road-cut. These include: volcanogenic clays (V1), jig-saw fractured blocks-containing debrites (V2), laminated limestone (F1a), massive limestone (F1b), laminated diatomite (F2a), and massive (opalised) diatomite (F2b).

The exposure is dominated by bedded clays of discrete colours ranging from light yellows, ochres, reddish brown to greenish grey (V1). The thickness of individual beds ranges from 1 to 10 cm (Figure 2B). Despite the actual clayey nature of these deposits, the textures of some beds suggest coarser grain-size (sandy), affected by post-depositional argillisation. These authigenic clays contain abundant clayey pseudomorphs after pyroxene. These bedded deposits are subhorizontally layered onto the outcrop periphery (undeformed sediments—s, Figure 2B), whereas in the central part, they are intensively deformed with detailed folding (deformed sediments—ds, Figure 2C). The highly deformed sediments surround chaotic debrites (V2).

The volcanogenic debrites (agglomerates, V2) occur mainly in the central part of the outcrop, but are present also as smaller 'windows' exposed within the deformed sediments (Figure 2A). The debrites (d in Figure 2A,D) are poorly sorted and matrix supported. The sub-rounded clasts consist of various types of volcanic rocks (alkaline basaltic rocks) up to 25 cm in size. Apart from the sub–rounded clasts, the debrites contain jig-saw fractured blocks or boulders (m in Figure 2A,D), which exceed the outcrop height (5 m) in size. These blocks are not coherent, but have a shattered structure with the jig-saw fit of the subgrains and matrix migrated into the block along subgrain boundaries (Figure 2E).

The laminated limestone facies (F1a) comprises millimetre-scale laminae or thin layers (3–20 cm; Figure 3A). Laminae are flat to undulating with small amplitude (Figure 3B) and very regular. Limestone disintegrates along

20554877, 2023, 4, Downloaded from https://onlinelibrary.wiley.com/doi/10.1002/dep2.240 by Cochrane Hungary, Wiley Online Library on [05/12/2023]. See the Terms and Conditions (https://onlinelibrary.wiley.com/terms-and-conditions) on Wiley Online Library for rules of use; OA articles are governed by the applicable Creative Commons License

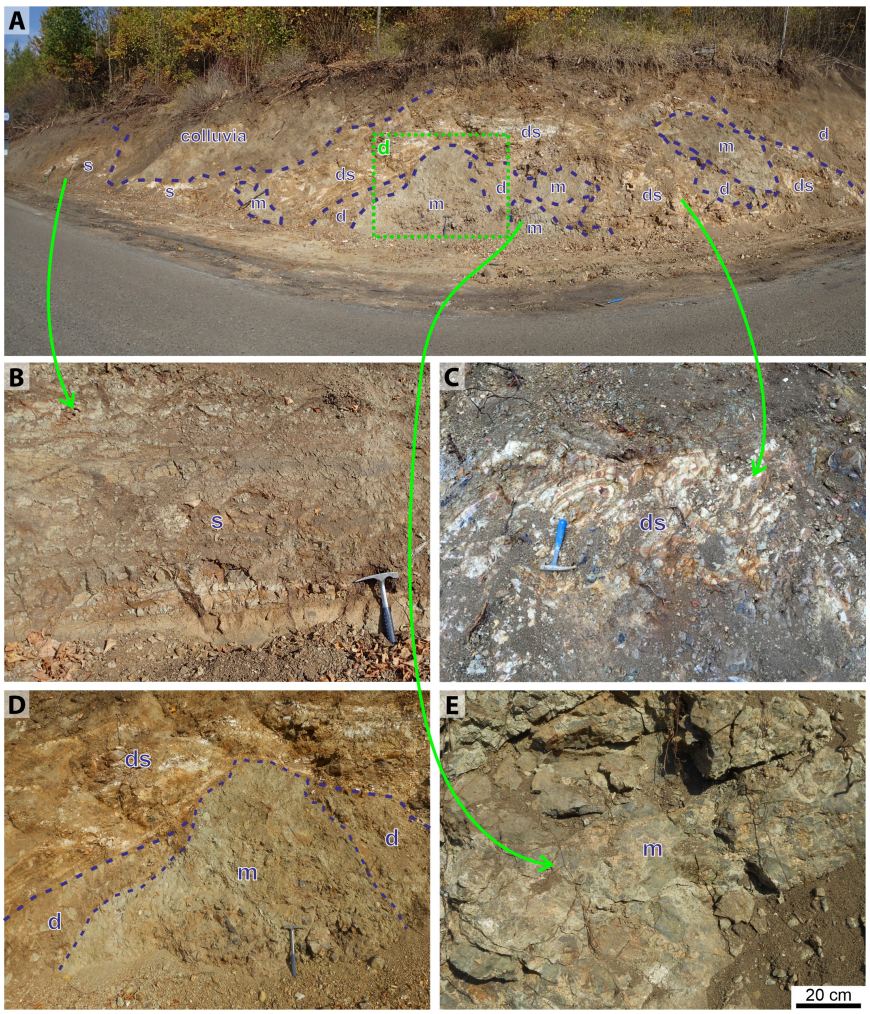

FIGURE 2 Volcaniclastic and sedimentary rocks exposed in the Dubina road-cut. (A) Overall view of the major part of the Dubina road-cut. (B) Subhorizontal planar bedding of weakly to undeformed sedimentary sequence (s) comprising mainly colourful volcanigenic clays. (C) Close-up of intensively deformed stratified sediments (ds). (D) Contact between jig-saw fractured blocks-containing debrite (debris avalanche deposit) and deformed sediments. (E) Close-up of jig-saw fit texture of subgrains within a jig-saw fractured block (m). d = debrite, ds = deformed sediments, m = jig-saw fractured block, s = sediments.

these laminae into 1–2 mm thin plates. The rock resembles planar stromatolites, but lacks fibrous structures perpendicular to the lamination (indicative of stromatolite fabrics, cf. Martin-Bello et al., 2019). Light-coloured laminae (1.5–2.0 mm thick) alternate with dark laminae/interlaminae (0.1–0.5 mm), which locally pinch out. Individual light laminae are formed by microsparite without visible fossils and are very homogenous. Size gradation of crystals within light laminae may be present. Dark laminae are not well defined and they are formed by amorphous organic matter and iron oxides and a mixture of clay minerals (probably montmorillonite group; Figure 3C) generating a honey yellow to brown mass resembling amorphous silica. Detrital micas (up to 0.8 mm) appear rarely, and are oriented parallel to lamination. Dark organic matter and iron oxides (diagenetic products; interpreted here as remnants of microbial mats) are present locally. Admixed clastic material is very rare and this is represented by monocrystalline and polycrystalline quartz (up to 0.25 mm). Microsparite occurring near interlaminar joints recrystallised into coarser grained sparite. Interlaminar joints or dark laminae are commonly lined with these rhombohedral crystals, accumulating somewhere inside the dark laminae.

Massive limestone facies (F1b) are usually present as lenses (up to 12 cm thick), macroscopically grey and finely crystalline. They are massive, mostly microsparitic (only locally micritic; Figure 3D) and admixed with mica. Typical of this facies are oblique structural domains resembling stylolites or cleavage (Figure 3E,F), which indicate significant deformation. Small lenses (*ca* 1 mm long) of microsparite calcite crystals are structurally limited (Figure 3F). These lenses resemble laminae facies F1a. All massive F1b limestones lack bioturbation and they are palaeontologically sterile.

Diatomites are described for the first time at the DHVC. Their origin can be safely assumed to be similar to occurrences in other parts of the Ohře (Eger) Rift, for example the Eocene–Oligocene Kučlín and Bechlejovice palaeontological sites in the České Středohoří Volcanic Complex (Bellon et al., 1998; Kvaček, 2002; Mach & Dvořák, 2011), or the Lower Miocene Cypris Formation in the Sokolov Basin (Rojík, 2013). Diatomite facies in the Dubina section are exposed in their original position under the debrite accumulation, and as fragments inside the debrite body (as rip-up clasts). Diatomite generally predominates over limestone in the exposed profile.

Laminated diatomite facies (F2a, Figure 4A) are very light in colour, usually light grey to ochre, porous, thin layers (usually

20554877, 2023, 4, Downloaded from https://onlinelibrary.wiley.com/doi/10.1002/dep2.240 by Cochrane Hungary, Wiley Online Library on [05/12/2023]. See the Terms and Conditions (https://onlinelibrary.wiley.com/terms-and-conditions) on Wiley Online Library for rules of use; OA articles are governed by the applicable Creative Commons License

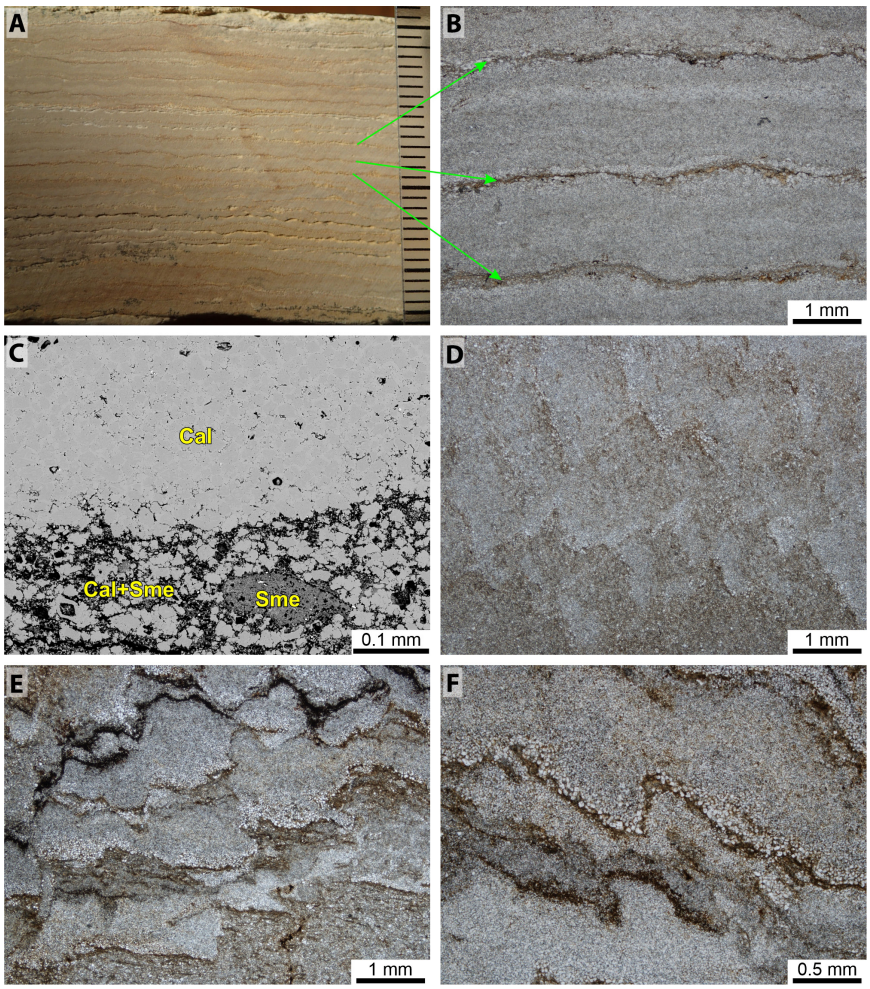

FIGURE 3 Carbonate sediments from Dubina road-cut. (A) Laminated limestone in polished section, mm-scale laminas are laterally constant (each mark on the scale represents 1 mm). (B) Detail of laminae in thin section (the same sample as in photograph A), very regular laminae are flat to undulating with small amplitude, dark interlaminae that are locally reduced. (C) Back-scattered electron image showing detail of light and dark laminae, Cal = calcite, Sme = smectite. (D) Massive micritic limestone with 'ghost' stylolite-type structures, thin section. (E) Oblique structural domains resembling stylolites or cleavage, thin section. (F) Detail of stylolite-type structure with structurally limited microsparite domains, thin section.

up to 7 cm), that do not contain a macro-palaeontological record. Massive opalised fragments (F2b, Figure 4B) are also classified as diatomites with their amorphous character representing a specific subfacies. Individual collected fragments of this rock type reach several decimetres in diameter. The colour varies from dark brown in the cores of individual boulders to a whitish crust (Figure 4B), which may reflect weathering. Distinguishable diatom valves are missing. Intensively wrinkled fine lamination is visible in some samples (Figure 4C,D,E). Silicified rhombohedral crystals are visible under the microscope (Figure 4F). The wrinkled lamination is remarkably similar to laminated diatomite (F2a, Figure 4A), including large crystals of sparite, but secondarily silicified. Ptygmatically folded cracks are also secondarily filled with chalcedony.

4.1.2 | Sedlečko section

The more peripheral (more distant from the centre of the volcano) facies of the investigated sedimentary system were exposed in Sedlečko village (Figure 1C), where sparitic (F3) and brecciated travertine facies (F3a) were uncovered in excavations for home construction. Block samples of both lithofacies were gathered, but a sedimentary profile is lacking. In a nearby abandoned limestone quarry (Figure 1C), however, a transition from fine-grained volcanoclastic debrites (V3) to micritic limestone (lacustrine) and travertine (spring) (F3 and F4) was documented. In addition, laminated lithographic limestones have been reported in the literature (Reuss, 1854, 1863; Reuss & von Meyer, 1849). Here, the term travertine is used in its broadest sense, comprising all non-marine carbonate precipitates in or near terrestrial springs, rivers, lakes and caves (sensu Fouke et al., 2000; Sanders & Friedman, 1967). This concept does not take into account the water temperature, contrary to the classification scheme of Glover and Robertson (2003) whose work defined travertine as hot-spring deposits from water temperatures >20°C. The moderate primary porosity and dendritic fabric of the studied samples are characteristic of travertine according to Flügel (2004).

Lithofacies F3 comprises sparite to microsparite limestone with conspicuous travertine textural features (Figure 5A through D). Macroscopically, it commonly developed as grey rocks with a dendritic fabric and nodular surfaces (Figure 5C). Locally, it displays horizontal lamination. The more prevalent nodular domains, without the laminar

20554877, 2023, 4, Downloaded from https://onlinelibrary.wiley.com/doi/10.1002/dep2.240 by Cochrane Hungary, Wiley Online Library on [05/12/2023]. See the Terms and Conditions (https://onlinelibrary.wiley.com/terms-and-conditions) on Wiley Online Library for rules of use; OA articles are governed by the applicable Creative Commons License

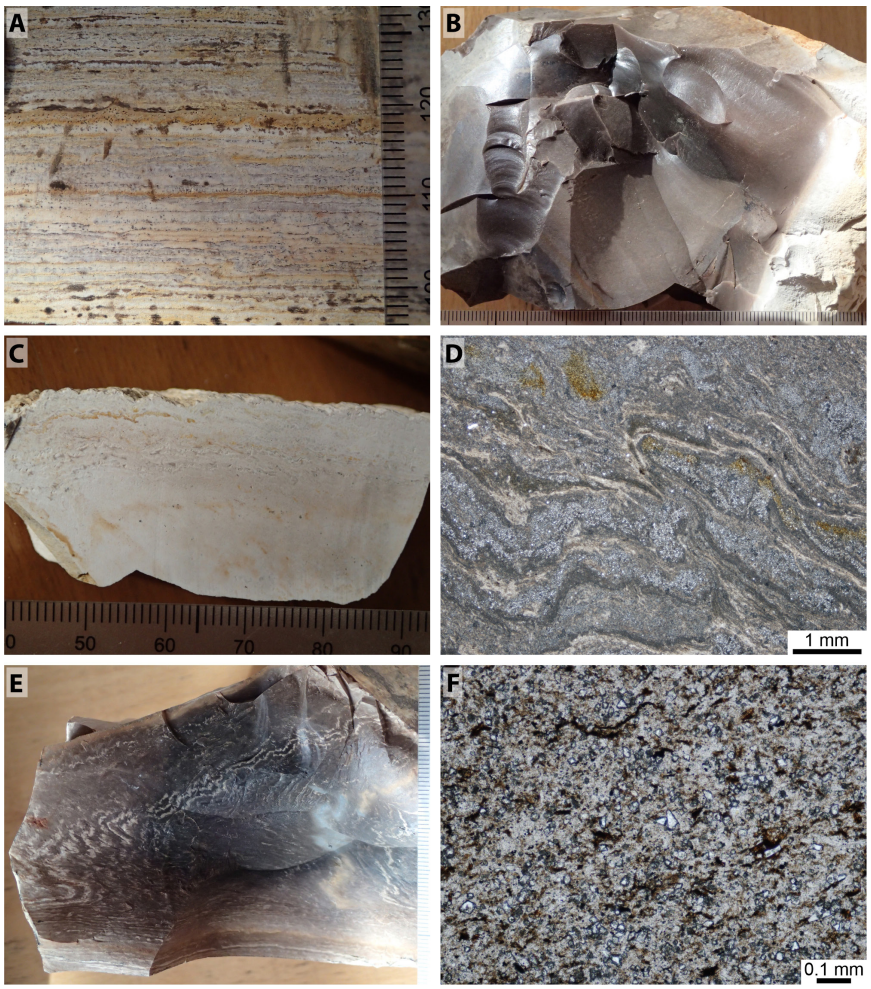

FIGURE 4 Diatomites from Dubina road-cut. (A) Laminated diatomite with regular lamination (F2a). (B) Opalised fragment with massive (amorphous) character, the colour varies from a dark brown in the cores of individual boulders to a whitish crust. (C) Intensively wrinkled fine lamination, macroscopic view. (D) Intensively wrinkled fine lamination in thin section, same sample as in photograph C. (E) Sample of amorphous opalised diatomite fragment with visible remains of wrinkled lamination. (F) Thin section of massive diatomite with silicified calcite or dolomite rhombohedral crystals inside microcrystalline to cryptocrystalline matrix. Each mark on the scale represents 1 mm.

structures, resemble calcareous tufa. They are more porous than their laminated counterparts, and probably represent travertines with cauliflower-like structures (sensu Chafetz & Folk, 1984; Koutecký et al., 2019). Some samples have a dendritic fabric resulting from carbonate encrustation of plants (Figure 5B,D). Remains of fossils are represented only by rare and small fragments of plant leaves and stems or indeterminate reed fragments. A special subtype of lithofacies F3 is represented by brecciated travertine (F3a). This type of limestone occurs as blocks in slope deposits encountered in the excavation. The blocks seem to represent disintegrated variably sized lenses of travertine characterised by brecciated structure at micro-scale (Figure 5E), and to a limited extent, also at the macro-scale (in the limestone quarry, the microbreccias occur only rarely). Remnants of micritic shrubs and secondary silicification in pore spaces are present (Figure 5F). The F3 limestone contains secondary iron oxides and a clay admixture. This type of limestone is very rich in fossil remains, especially gastropods and reed fragments.

The micritic to microsparitic limestone lithofacies (F4) is developed as a grey homogenous, locally laminated deposit (Figure 5A). It may also be partly porous at a micro-scale. This micro-porosity is probably the product of secondary dissolution of carbonate material (mostly sparite). The laminae may represent (seasonal) fluctuations in the contribution of carbonate material. Fossil remains, especially leaf imprints, are rare. Lastly, a now-depleted calcareous lithofacies, lithographic limestone (F5) was also present in the study area. This, however, was fully exploited and is not preserved. From descriptions in the literature, in both localities it was fine-grained, yellowish in colour and contained abundant leaf imprints. Its fine lamination resulted in platy fracture enabling the use of this limestone for lithographic purposes (Glückselig, 1842).

The fine-grained debrite lithofacies (V3) is exposed on the eastern margin of the Sedlečko limestone pit. It differs from the Dubina road-cut (V2 facies) in its significantly finer grain-size (Figure 6A) and absence of jig-saw-fragmented blocks. The deposits comprising the debrite facies are poorly sorted, matrix-supported, with a sandy to silty matrix significantly predominating over small and well-rounded pebbles. The pebbles do not exceed 7 cm in diameter (mostly around 3–5 cm, Figure 6B), and consist of various types of alkaline basaltic lavas. Poor sorting and moderate rounding can be also observed in the groundmass under microscopic

20554877, 2023, 4, Downloaded from https://onlinelibrary.wiley.com/doi/10.1002/dep2.240 by Cochrane Hungary, Wiley Online Library on [05/12/2023]. See the Terms and Conditions (https://onlinelibrary.wiley.com/terms-and-conditions) on Wiley Online Library for rules of use; OA articles are governed by the applicable Creative Commons License

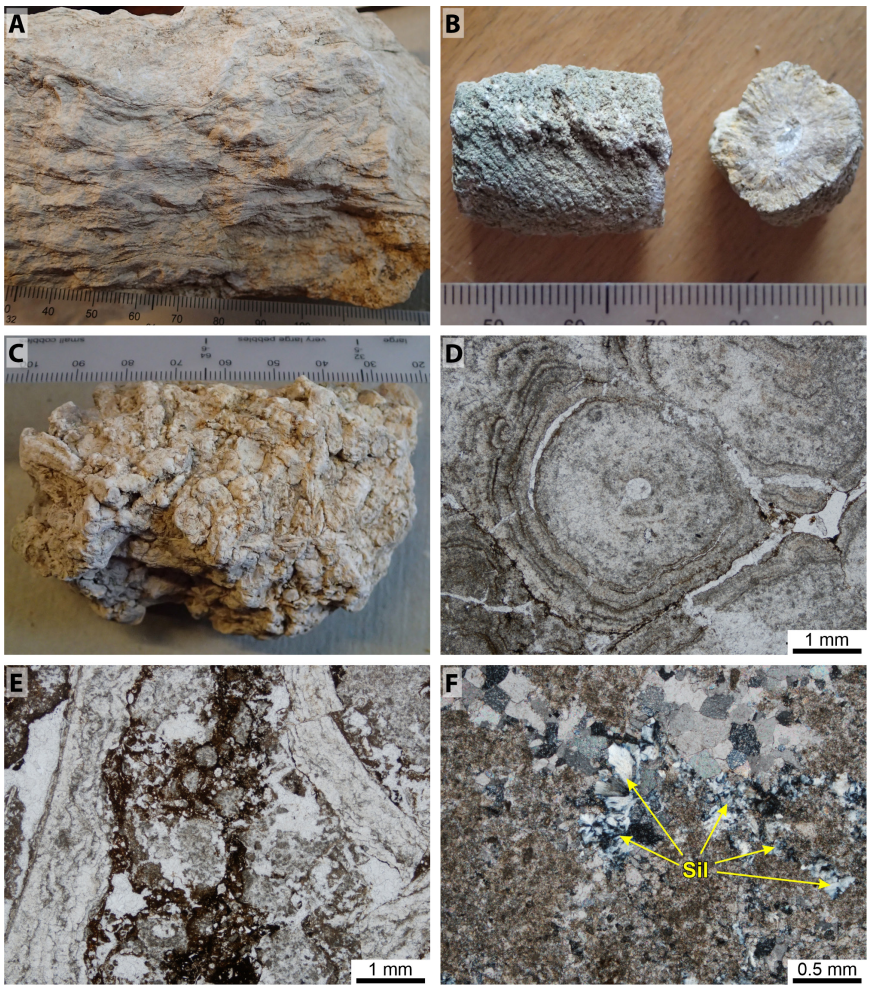

FIGURE 5 Limestones from Sedlečko outcrops. (A–D) Sedlečko abandoned limestone quarry. (E and F) Temporary excavations for family house. (A) Thin laminated micritic limestone. (B) Encrusted bioclast (reed or twig fragment) with dendritic fabric. (C) Typical shrub-like structure probably supported by bacterially induced precipitation or by growth of bryophyte. (D) Internal structure of travertine in thin section, internal concentric growth lines usually formed around the bioclasts. (E) Brecciated travertine with higher content of iron oxides. (F) Secondary silicification (Sil) partly affecting the calcite sparite crystals and micritic matrix with clay admixture. Each mark on the scale represents 1 mm.

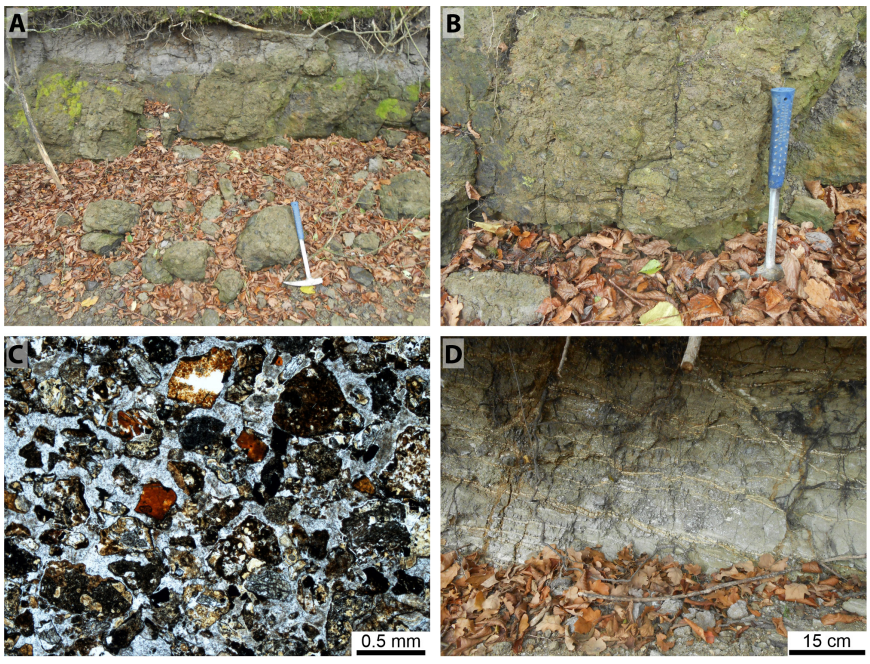

FIGURE 6 Volcanoclastic agglomerate (debrite) exposed at Sedlečko (V3 facies). (A) Poorly sorted matrix-supported fine-grained debrite at Sedlečko. (B) Close-up of small volcanic pebbles enclosed in the sandy matrix. (C) Microphotograph of the poorly sorted debrite groundmass with moderately to poorly rounded sand-sized clasts of various basaltic rocks. (D) System of post-depositional carbonate veins cross-cutting the debrite accumulation.

investigation (Figure 6C). The agglomerate (probably two depositional units, with a poorly developed boundary) is crosscut by a system of post-depositional carbonate veins (Figure 6D). These veins are mostly subhorizontal, and their frequency increases from east (debrite source) to west (centre of the limestone pit).

20554877, 2023, 4, Downloaded from https://onlinelibrary.wiley.com/doi/10.1002/dep2.240 by Cochrane Hungary, Wiley Online Library on [05/12/2023]. See the Terms and Conditions (https://onlinelibrary.wiley.com/terms-and-conditions) on Wiley Online Library for rules of use; OA articles are governed by the applicable Creative Commons License

4.2 | Elemental and C-O-Sr isotope geochemistry

Five representative calcareous samples were investigated spectroscopically with regard to their major oxide, minor and trace element, stable C and O and radiogenic Sr isotope compositions. The sample set was obtained at the (i) Dubina road-cut ($n=2$), (ii) Sedlečko limestone pit ($n=2$), and (iii) Sedlečko excavation ($n=1$). Analyses revealed a calcitic composition with relatively low MgO (0.2–1.1 wt%), FeO (0.1–1 wt%), and MnO contents (0.1–0.3 wt%; Table 1; Figure 7A). The samples contain notable amounts of SiO_2 (0.6–2.6 wt%), with a positive correlation between SiO_2 and TiO_2 (Figure 7B) suggestive of basaltic silt admixture. The only exception is one sample from Sedlečko limestone pit (Sed-I_01), where no TiO_2 was detected.

The chondrite-normalised (Boynton, 1984) REE patterns (Figure 7C) are characterised by smooth and relatively flat patterns with generally very low REE contents (ΣREE = 2.6–27 ppm). The lowest REE concentrations were detected in sample Sed-I_01, which is also characterised by uncoupled SiO_2–TiO_2. The analysed limestone samples display a negligible Eu anomaly, except for sample DR339 of the brecciated travertine (F3a) facies that probably represents a spring-outpouring site. Sample DR339 displays a slight positive Eu anomaly ($Eu_N/Eu_N^* = 1.35$). When the extended set of trace elements is normalised to an average representative of DHVC basaltic lavas (after Rapprich & Holub, 2008), significant depletion in all elements, except for U, Sr and P is observed (Figure 7D).

The measured $\delta^{13}C$ and $\delta^{18}O$ values are listed in Table 2, and shown in Figure 8. With $\delta^{13}C$ isotope values ranging from −1.0‰ to 2.2‰, the samples fall within the mode observed for 90% of travertine deposits (Pentecost, 2005). The lowest measured value occurs in sample Dub_02, followed by brecciated travertine sample DR339, with similarly positive values observed in samples representative of both localities (Table 2). The $\delta^{18}O$ values of the samples are in the 19.9%–23.0‰ range and display relatively ^{18}O-enriched values at the Dubina proximal site. If one considers the travertine-depositing waters to be mainly, but not entirely, of meteoric origin, and thus exhibiting a palaeo- $\delta^{18}O$ value somehow similar to that of modern day stream waters in the Karlovy Vary (Carlsbad) region, which fluctuate on a yearly-basis between −11.0‰ and −8.4‰ (Buzek et al., 1991), then an equilibrium deposition temperature of between 10 and 23°C can be derived. This estimate applies the quadratic equation relating δc and δw with temperature, as first devised by O'Neil et al. (1968), and revised by Hays and Grossman (1991). Depletion in ^{18}O in the measured samples occurs in parallel with a ^{13}C enrichment.

Strontium isotopic data for the studied carbonates are presented in Table 3 and Figure 9, together with previously published data for basaltic lavas (a possible source of calcium), leachates and residuals of these basaltic samples and hot-spring travertines from Karlovy Vary. Sedimentary carbonates from Dubina and Sedlečko show rather homogeneous $^{87}Sr/^{86}Sr$ isotopic compositions. The limestone sample from the construction site in Sedlečko (DR339) and the limestones from Dubina (Dub_01 and Dub_02) show strikingly non-radiogenic values of $^{87}Sr/^{86}Sr$ (0.7038, 0.7041 and 0.7039 respectively), while the two samples from Sedlečko quarry (Sed-I_01 and Sed-I_02) have slightly elevated $^{87}Sr/^{86}Sr$ values (0.7046 and 0.7049). In contrast, travertines from the recent Karlovy Vary hot-spring (Vylita & Žák, 2009) are characterised by significantly more radiogenic $^{87}Sr/^{86}Sr$ values (0.7191–0.7199).

As the alkaline basalts of the DHVC are rich in CaO (9–15 wt%; Rapprich & Holub, 2008), weathering of these rocks may provide enough CaO for carbonate precipitation at the volcano foothills. The weathering and CaO release may be facilitated by fragmentation of the basaltic rocks, leading to increased reaction surfaces. To test this hypothesis, leaching experiments of four representative basaltic lavas and a lahar deposit were carried out. The leachate and residuum of lahar samples collected on the edge of the Sedlečko limestone pit display only a small difference, having $^{87}Sr/^{86}Sr$ values of 0.7048 and 0.7049 respectively. Higher variability can be observed in the case of basaltic lavas with leachates characterised by slightly more radiogenic values (0.7045–0.7049) than the residuum (0.7042–0.7047; Table 3).

4.3 | Fossil associations

Three taxa of freshwater gastropods were distinguished in Sedlečko limestones, that is, *Lymnaea* sp., *Stagnicola* sp. (Figure 10A,B), and *Radix* sp. (Figure 10C,D,E) representing the Lymnaeidae family (pond snails). In addition, several individuals of *Planorbis* sp. from the Planorbidae family (ramshorn snails) were also found (Figure 10F,G). Several individuals could not be classified due to shell dissolution and preservation of the shell-core only (Figure 10H). In other cases, the gastropod shells had been shattered by compaction (Figure 10I,J). The relatively low diversity gastropod fauna is accompanied by a monospecific ostracod fauna represented by a single species *Virgatocypris* cf. *virgata*. The genus *Virgatocypris* is known to occur since the Late Cretaceous, but *Virgatocypris virgata*, in particular, is commonly recorded from the Upper Oligocene to Early Miocene lacustrine successions of Europe (Pokorný, 1986; Witt, 2001, 2002) and Turkey (Agbulut et al., 2020).

The fossil fauna is accompanied by numerous remnants of fossil flora, despite many of these remnants being too fragmented or incomplete for taxonomic classification. Volcaniclastic siltstones occur as thin layers atop individual

20554877, 2023, 4, Downloaded from https://onlinelibrary.wiley.com/doi/10.1002/dep2.240 by Cochrane Hungary, Wiley Online Library on [05/12/2023]. See the Terms and Conditions (https://onlinelibrary.wiley.com/terms-and-conditions) on Wiley Online Library for rules of use; OA articles are governed by the applicable Creative Commons License

TABLE 1 Chemical composition of studied freshwater limestones.

Sample	Dub_01	Dub_02	Sed-I_01	Sed-I_02	DR339
Locality	Dubina	Dubina	Sedlečko	Sedlečko	Sedlečko
Rock	Limestone	Limestone	Limestone	Limestone	Brecciated travertine
SiO_2	1.82	2.58	2.42	0.61	1.13
TiO_2	0.09	0.13	<0.01	0.05	0.07
Al_2O_3	0.36	0.70	0.15	0.32	0.25
Fe_2O_3	1.56	0.60	0.34	0.52	2.63
FeO	0.99	0.20	0.92	0.79	0.17
MgO	1.07	0.52	0.20	0.24	0.86
MnO	0.206	0.199	0.187	0.105	0.284
CaO	50.47	51.24	52.80	53.35	51.09
Na_2O	0.06	0.04	<0.01	0.01	0.04
K_2O	0.08	0.56	0.01	0.03	0.04
P_2O_5	0.040	0.133	0.168	0.099	0.342
F	0.156	0.058	0.019	0.020	0.274
CO_2	39.63	39.92	42.00	42.72	40.75
C(org.)	1.216	0.631	0.110	0.136	0.273
S(tot.)	0.070	0.064	<0.010	0.011	0.201
$H_2O(+)$	2.02	1.18	<0.05	<0.05	0.73
$H_2O(-)$	0.33	0.24	0.10	0.26	0.28
Total	100.36	99.18	99.30	99.17	99.56
Cr	5.0	10.9	5.5	5.9	8.5
Ga	1.2	5.4	0.26	1.0	0.81
Hf	0.69	0.33	0.21	0.25	0.57
Nb	<1.0	2.7	<1.0	5.5	3.0
Ni	4.3	4.8	3.5	3.4	10.7
Pb	<0.5	<0.5	<0.5	<0.5	<0.5
Rb	1.6	7.6	0.9	2.8	1.5
Ta	<5.0	<5.0	<5.0	<5.0	<5.0
Th	0.15	0.22	0.11	0.16	0.32
U	1.6	4.8	1.4	2.0	6.4
V	59	47	25	45	35
Y	2.6	2.0	0.64	5.3	2.8
Zr	71	18	27	25	73
Sr	1706	1480	335	414	1116
Sc	1.5	2.6	<1.0	2.2	1.9
Ba	178	174	24	40	292
La	2.8	4.5	0.67	6.0	3.1
Ce	4.8	8.3	1.0	10.6	3.8
Pr	0.55	1.0	0.13	1.3	0.51
Nd	2.1	3.7	0.43	4.9	1.8
Sm	0.35	0.63	0.08	0.90	0.31
Eu	0.12	0.22	0.03	0.29	0.13

(Continues)

20554877, 2023, 4, Downloaded from https://onlinelibrary.wiley.com/doi/10.1002/dep2.240 by Cochrane Hungary, Wiley Online Library on [05/12/2023]. See the Terms and Conditions (https://onlinelibrary.wiley.com/terms-and-conditions) on Wiley Online Library for rules of use; OA articles are governed by the applicable Creative Commons License

TABLE 1 (Continued)

Sample	Dub_01	Dub_02	Sed-I_01	Sed-I_02	DR339
Locality	Dubina	Dubina	Sedlečko	Sedlečko	Sedlečko
Rock	Limestone	Limestone	Limestone	Limestone	Brecciated travertine
Gd	0.36	0.52	0.07	0.90	0.28
Tb	0.05	0.07	0.01	0.13	0.04
Dy	0.26	0.34	0.05	0.78	0.20
Ho	0.05	0.06	<0.02	0.16	0.04
Er	0.16	0.16	0.05	0.43	0.12
Tm	0.02	0.02	0.01	0.06	0.02
Yb	0.15	0.14	0.07	0.38	0.10
Lu	0.03	0.02	0.02	0.05	0.02

Note: Major oxides in wt.%, trace elements in ppm.

flow units of debrites (debris flow and debris avalanche deposits). In Dubina, these contain abundant leaves of *Platanus neptuni* (Figure 11A). Leaves and stipules of this tree can also be found in Dubina limestones (Figure 11B), along with leaves of *Populus* sp. (Figure 11C), *Acer* cf. *tricuspidatum*, *Daphnogene cinnamomifolia* form *lanceolata*, *Alnus* sp., and fragments of other undetermined angiosperm leaves (possibly *Dicotylophyllum* sp.). Conifer remnants were found solely in diatomite, represented by strobili, probably of *Calocedrus* sp.

Fine-grained facies associated with distal lahars at Sedlečko contain imprints of leaves of *Engelhardia orsbergensis*, *Rumohra recentior* and *Eotrigonobalanus furcinervis* (Figure 11D). The latter occurring also in the limestones along with *Laurophyllum* sp., *Dombeyopsis lobata*, *Craigia bronii* (Figure 11E) and *Alnus* sp. (Figure 11G). Genus *Alnus* is represented also by calcified wood *A. tschemrylica* (Figure 11F). Randomly or radially oriented calcite straws correspond to reed-bunches (Figure 11H,I).

4.4 | Geochronology

To better constrain the timing of the studied sequence, geochronological analyses were carried out on two lava samples, DB02 and DR334, interbedded and overlaying the sequence respectively (Figure 1C; Table 4). The aphanitic tephrite lava (sample DB02) is embedded in the debrite sequence near the documented road-cut in Dubina. This lava occurs *ca* 10 m up the slope above the studied sediments, deformed by debris avalanche indention. Two fractions prepared from this lava sample, representing both the bulk-rock and the light groundmass, provided almost identical age results of 25.04 ± 0.36 and 25.34 ± 0.36 Ma respectively (Chattian, late Oligocene; Table 4). The difference does not exceed analytical error. Taking rapid deposition of the volcanoclastic debrites and the span of analytical error into account, the obtained ages refer to the deposition of the agglomerate fan. In the area between the studied outcrops at Dubina and Sedlečko, other lava is exposed (Figure 1C). Unlike the tephrite DB02, the lava of the porphyritic trachybasalt DR334 fills a palaeovalley developed in the debrites, but orientated perpendicular to the general trajectory seen in the lahars. Age determination of this lava flow yields 21.64 ± 0.31 Ma (Aquitanian, early Miocene; Table 4).

5 | DISCUSSION

5.1 | Age of the studied succession

Due to poor preservation, the zoopalaeontological material provides insufficient background for chronostratigraphic interpretations. Concerning the fossil flora, the co-occurrence of *Eotrigonobalanus* (Figure 11E) with *Craigia* (Figure 11F) and *P. neptuni* (Figure 11A,B) points to the early to late Oligocene floral assemblage Nerchau-Florsheim sensu Mai (Kvaček & Walther, 2001), and relates the flora described here with that of Suletice from the České Středohří Mountains (Kvaček & Walther, 1995, 2003). The geochronological data from the tephrite lava DB02 (25.04 ± 0.36 and 25.34 ± 0.36 Ma; Table 4) also place the studied succession in the Late Oligocene. The porphyritic trachybasalt DR334 lava erupted in the early Miocene (21.64 ± 0.31 Ma; Table 4), but was emplaced onto the eroded relief of an agglomerate fan. In addition, the DR334 lava erupted from local fractures on the rift scarp and transected the agglomerate accumulations almost perpendicularly (*ca* N–S) to the debris flows trajectory (from east; Figure 1C). It is therefore assumed that a significant time-gap exists between deposition of agglomerates and eruption of the DR334 lava. Taking the position of both lavas into account, the Late Oligocene age is accepted.

20554877, 2023, 4, Downloaded from https://onlinelibrary.wiley.com/doi/10.1002/dep2.240 by Cochrane Hungary, Wiley Online Library on [05/12/2023]. See the Terms and Conditions (https://onlinelibrary.wiley.com/terms-and-conditions) on Wiley Online Library for rules of use; OA articles are governed by the applicable Creative Commons License

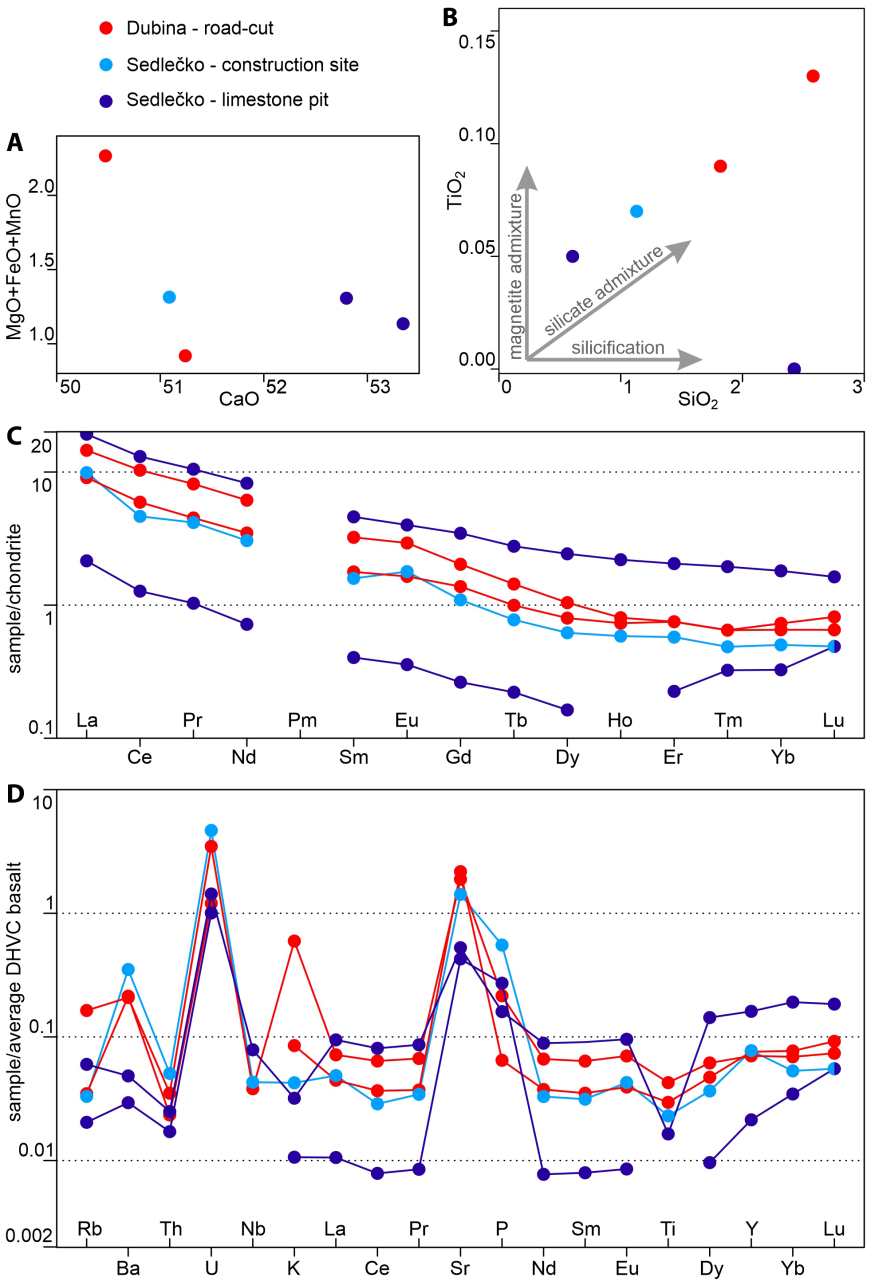

FIGURE 7 Carbonate geochemistry. (A) CaO versus FeO + MnO + MgO binary diagram. (B) SiO_2 versus TiO_2 binary diagram. (C) Chondrite-normalised (Boynton, 1984) REE contents. (D) Concentrations of expanded trace elements normalised to composition of DHVC basalts (average from Rapprich & Holub, 2008).

TABLE 2 C-O stable isotopes of studied freshwater limestone.

Sample	Sed-I_01	Sed-I_02	Dub_01	Dub_01 repeat	Dub_02	DR339
$\delta^{13}C$ (‰ V-PDB)	1.7	2.2	2.2	2.2	−1.0	0.8
$\delta^{18}O$ (‰ V-SMOW)	20.9	19.9	21.6	21.7	21.7	23.0

5.2 | Palaeoclimate and depositional environment

The floral assemblage can be characterised as a warm-temperate to subtropical mixed mesophytic forest (MMF) to subtropical broad-leaved evergreen forest (BLEF; Teodoridis & Kvaček, 2015). Subtropical conditions would have been beneficial for chemical weathering of volcanic and volcanoclastic rocks. Insufficient preservation of the collected fossils precludes detailed determination and taxonomical categorisation, but it is sufficient for a palaeoecological estimation. The present species point to a habitat of shallow standing or slowly running freshwaters on a muddy substrate, which may include ponds or temporarily drying flood water bodies (Flügel, 2004). Some limestone samples have a dendritic fabric resulting from carbonate encrustation

20554877, 2023, 4, Downloaded from https://onlinelibrary.wiley.com/doi/10.1002/dep2.240 by Cochrane Hungary, Wiley Online Library on [05/12/2023]. See the Terms and Conditions (https://onlinelibrary.wiley.com/terms-and-conditions) on Wiley Online Library for rules of use; OA articles are governed by the applicable Creative Commons License

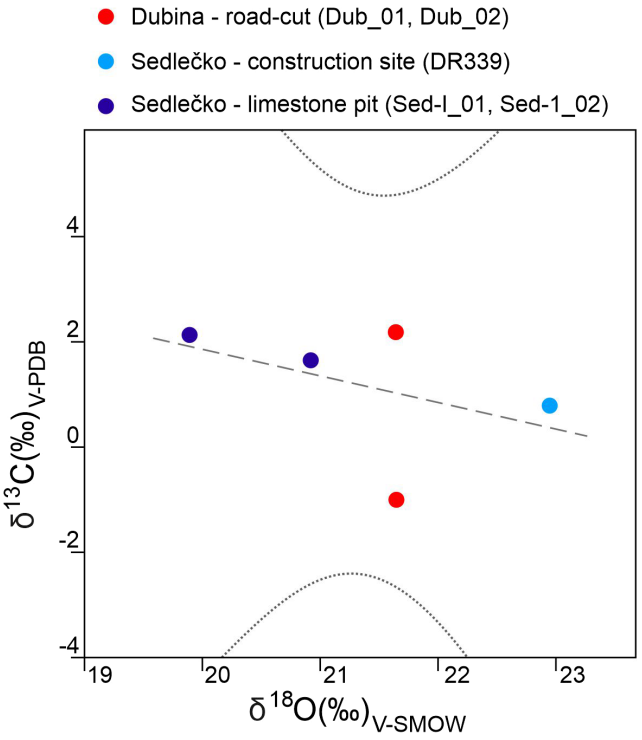

FIGURE 8 Cross-plot of $\delta^{13}C$ (‰) versus $\delta^{18}O$ (‰). The linear correlation of the model is not significant ($r^2 = 0.181$) and the model is strongly biased by sample DR339 (standardised residual = −1.47). The 99% confidence range is also displayed.

of plants (Figure 5B,D), and would have formed close to a spring, or at the shore of a carbonate-oversaturated shallow lake (sensu Pentecost & Viles, 1994). The molluscs and terrestrial gastropods are usually very restricted to certain habitats. The species composition of the gastropod community, that is, a combination of their ecological requirements, is a very accurate ecological indicator of the environment at a specific locality. Palaeoenvironmental reconstruction presented here compare to that of palaeontological localities at Sandelhausen (Southern Germany, Early/Middle Miocene; Moser et al., 2009), and Lapsarna (Western Lesvos, Greece, Early Miocene; Vasileiadou et al., 2017). The recent representatives of the Lymnaeidae family, genera *Stagnicola*, *Lymnaea* and *Radix* inhabit standing waters, such as lakes and ponds, swamps and marshes. The genus *Radix* indicate peaty waters on muddy or stony ground near the bank of lakes, slowly flowing rivers and smaller and shallower water bodies. Some species can withstand drier conditions or short droughts. The recent species of *Planorbis* generally inhabit wetlands, pools or shallow and smaller ponds overgrown with macrovegetation, in standing or slowly flowing water. Palaeoecology of the fossil gastropod faunal assemblage from the Sedlečko locality was evaluated employing the ecological demands and distribution of closely related living species, as documented by Ložek (1964) and Kerney et al. (1983). The ostracod species *V. virgata* is usually part of the *Candona-Cypridopsis* assemblage, which is thought to have characterised a shallow lake or lake banks with water depths up to around 1 m (Malz & Moayedpour, 1973; Witt, 2002).

Intermittent (possibly seasonal) sedimentation in a shallow lake or periodically flooded marsh would also correspond to the finely laminated character of the limestone. The appearance of laminar limestone resembles calcrete, or palustrine facies. Calcretes are defined as secondary accumulations of calcium carbonate (low-Mg and high-Mg calcite) in near-surface settings, which result from the cementation and/or replacement of host material by the precipitation of calcium carbonate from soil water or ground water (Wright, 1990). Definition of palustrine deposits is complicated—there are several ecological, hydrological and sedimentary parameters that should be considered. After definition by Cowardin et al. (1979) palustrine wetlands must fulfil one or more of the following requirements: (i) the land supports predominantly hydrophytes, at least periodically; (ii) the substrate is predominantly undrained hydric soil, and the substrate is non-soil and is saturated with a water cover or covered by shallow water at some time during the growing season.

In the Dubina section, there is no evidence of soil water or ground water, bioturbation, roots or ostracods, any mud cracks, etc. Plant remains are scarce and dominated by angiosperm trees. Leaves of *P. neptuni* can be found in both fine-grained volcaniclastic siltstones derived from debrites and limestones (Figure 10A,B). The laminar structure of limestone facies F1a is interpreted here as cryptomicrobial. Sedimentary rocks present at the Dubina section represents infill of a shallow water sedimentary basin or separate basins (lakes, ponds or puddles) originated in front of the volcanic complex. This basin (or basins) was indented by the debris avalanche. The unknown original position and interrelationship of carbonate and siliceous sediment fragments may represent one or more sedimentary basins, developed independently.

Carbonate sedimentation at Sedlečko was more complex. The brecciated travertine from the excavation (Figure 5E) corresponds to formation from a spring exiting a low mound close to the lake (Pentecost & Viles, 1994). This locality probably represents the margin of a very shallow lake, probably developed as paludal deposits (Pentecost & Viles, 1994), where the carbonate originated as cement around plant (e.g. reed) tussocks. Brecciation of the limestones probably formed by desiccation and/or is related to long-rooted grass colonisation of an exposed mud (Freytet & Verrecchia, 2002). They are formed with irregular periodicity and by reworking of desiccation breccias (Freytet & Verrecchia, 2002). The limestone lithofacies from the abandoned quarry at Sedlečko likely represent the main shallow lake sediments with carbonate development, and it is in the central part of this lake where the variably sized lenses of lithographic limestone (unfortunately not preserved) may have locally developed.

20554877, 2023, 4, Downloaded from https://onlinelibrary.wiley.com/doi/10.1002/dep2.240 by Cochrane Hungary, Wiley Online Library on [05/12/2023]. See the Terms and Conditions (https://onlinelibrary.wiley.com/terms-and-conditions) on Wiley Online Library for rules of use; OA articles are governed by the applicable Creative Commons License

TABLE 3 Radiogenic Sr isotope systematics of studied freshwater limestones compared with potential sources.

Sample	Locality	Type	Rock	Rb (ppm)	Sr (ppm)	$^{87}Sr/^{86}Sr$	2S(M)
V7[a]	Úhošť	Bulk	Basanite	35.6	1042	0.704234	7
V7-L	Úhošť	Leachate				0.704722	8
V7-R	Úhošť	Residuum				0.704171	9
V9[a]	Úhošť	Bulk	Basalt	48.0	847	0.704666	10
V9-L	Úhošť	Leachate				0.704887	9
V9-R	Úhošť	Residuum				0.704694	10
V14[a]	Úhošť	Bulk	Picrobasalt	12.0	553	0.70413	10
V14-L	Úhošť	Leachate				0.704454	9
V14-R	Úhošť	Residuum				0.704150	10
V5[a]	Úhošť	Bulk	Basalt	30.0	600	0.704646	14
V5-L	Úhošť	Leachate				0.704884	7
V5-R	Úhošť	Residuum				0.704719	8
DH1330[b]	Doupov	Bulk	Melteigite	27.0	563	0.703823	10
DR051B[b]	Doupov	Bulk	Urtite	84.0	3352	0.703608	15
TV52~	Doupov	Bulk	Essexite	69.0	844	0.704384	13
Dub_01	Dubina	Bulk	Limestone	1.6	1706	0.704075	8
Dub_02	Dubina	Bulk	Limestone	7.6	1480	0.703889	10
DR339	Sedlečko	Bulk	Brecciated travertine	1.5	1116	0.703841	10
Sed-I_01	Sedlečko	Bulk	Limestone	0.9	335	0.704873	10
Sed-I_02	Sedlečko	Bulk	Limestone	2.8	414	0.704604	9
Sed-l Lahar-L	Sedlečko	Leachate	Lahar			0.704780	8
Sed-l Lahar-R	Sedlečko	Residuum	Lahar			0.704863	9
KV-A	Karlovy Vary	Bulk	Hot-spring limestone			0.719148	21
KV-B	Karlovy Vary	Bulk	hot-spring limestone			0.719879	9
KV-C	Karlovy Vary	Bulk	hot-spring limestone			0.719886	10
KV-D	Karlovy Vary	Bulk	hot-spring limestone			0.719936	8

[a]Data from Rapprich and Holub (2008).

[b]Data from Holub et al. (2010).

5.3 | Source of reactants for carbonate precipitation

5.3.1 | Stable carbon isotopes

To understand the source of reactants for carbonate precipitation, three independent isotopic systems were examined. The $\delta^{13}C$ values obtained (−1.0‰ to 2.2‰) fit into the modal range (−1‰ to 10‰) of travertine-fixed carbonate ions originated from a variable combination of pre-existing limestone decarbonation and fluid-rock exchange reactions. Magmatically derived CO_2 was also important (Pentecost, 2005). This conferred an isotopically lighter signature to the resulting travertine, which exhibits a mixed source of dissolved inorganic C. The absence of pre-existing limestones in this area and the position of the studied sites at the volcano periphery, away from the degassing volcanic conduits, reduces the list of potential sources. Nowadays CO_2 outflows along the Ohře Rift faults are also characterised by mantle-like $\delta^{13}C$ (*ca* −4‰; Mach et al., 2017), although no magmatic activity has occurred in the central segment of the rift since the Tortonian period, *ca* 10 Ma (Cajz et al., 2009). As the aqueous CO_2 phase containing a fraction of mantle-derived CO_2 approached atmospheric equilibrium, the resulting lake travertine carbonate precipitate would have become slightly enriched in ^{13}C.

20554877, 2023, 4, Downloaded from https://onlinelibrary.wiley.com/doi/10.1002/dep2.240 by Cochrane Hungary, Wiley Online Library on [05/12/2023]. See the Terms and Conditions (https://onlinelibrary.wiley.com/terms-and-conditions) on Wiley Online Library for rules of use; OA articles are governed by the applicable Creative Commons License

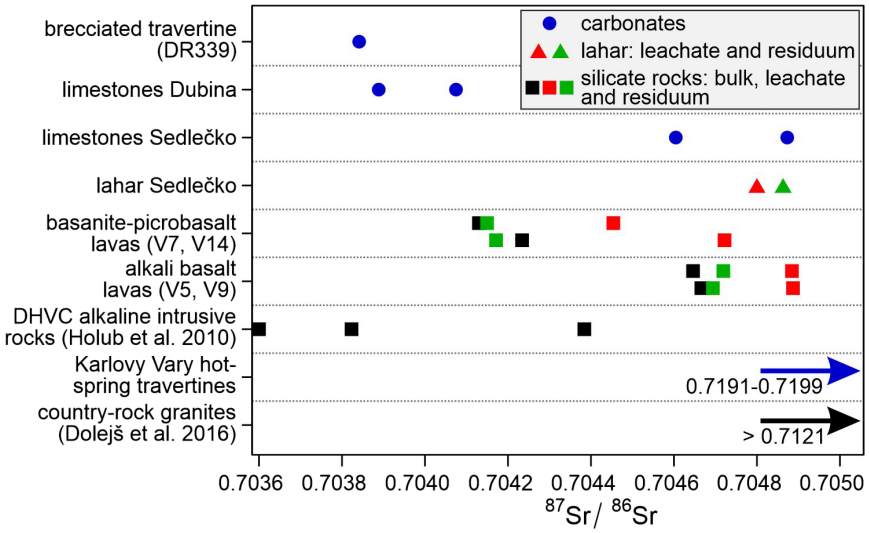

FIGURE 9 Sr isotopes of analysed limestones compared with DHVC lavas (Rapprich & Holub, 2008), their leachates and residuums, leachate and residuum of distal lahar deposit, DHVC intrusive rocks (Holub et al., 2010), Karlovy Vary hot-spring travertines (this study) and country-rock granites (Dolejš et al., 2016).

5.3.2 | Stable oxygen isotopes

Highly positive $\delta^{18}O$ values (19.9–23.0‰; Table 2) imply involvement of water highly affected by evaporation into building of carbonate ions. Such a scenario is in good agreement with palaeontological and sedimentological (e.g. Figure 3A) observations suggesting that ponds where limestone precipitated were ephemeral. Despite the fact that significant amounts of dolomite could be expected in limestones deposited in periodically evaporating ponds (Muir et al., 1980) and the surrounding basaltic lavas are rich in MgO (up to 12.5 wt%; Rapprich & Holub, 2008), only negligible amounts of dolomite were observed in the studied Oligocene limestone. This discrepancy can be explained by the character of the basaltic lavas weathering or the pH and alkalinity of the water in equilibrium with the precipitation environment. Formation of secondary iddingsite and smectite group minerals fixed large amounts of available MgO but almost no CaO, which remains mobile and soluble. Despite the elevated dissolved inorganic carbon levels, without a sustained alkaline generation and proton consumption mechanism also in place, calcite not dolomite would be favoured (Petrash et al., 2021).

5.3.3 | Radiogenic strontium isotopes

With the aim of confirming the hypothetical source of CaO from weathering of DHVC basaltic rocks and their volcaniclastics, several leaching experiments were carried out. During leaching of dry powders of fresh unaltered basaltic rocks at room temperature, the leachate yields a more radiogenic signature compared to bulk-rock and residuum (Table 3; Figure 9). In the case of fresh basaltic rocks, the low-temperature leaching preferably attacks the metastable phases (feldspathoids and glass) with a slightly more radiogenic signature. The opposite trend is observed in the case of the lahar deposit, where leachate provides a less radiogenic signature than the residuum (Figure 9). This trend possibly reflects the effect of long-term Oligocene weathering in subtropical conditions (Kvaček & Walther, 2001; Li et al., 2018), which occurred prior to fragmentation (triggering of the debris avalanche or debris flow) and continued also after its deposition. Such weathering leads to decomposition of mafic minerals first, namely olivine (Sr-poor) and clinopyroxene (Sr-rich).

In a magmatic system evolving through open-system processes (e.g. crustal contamination), isotopic ratios of the magmatic liquid from which crystals grow may change through time. Consequently, minerals (indeed growth zones within crystals) reflect the isotopic ratios of their environment at crystallisation; early-grown minerals may be different (e.g. less radiogenic $^{87}Sr/^{86}Sr$ in a system with progressive incorporation of crustal material) to later-crystallised phases. In a system where two magmatic components mix, crystal cores may record the isotopic character of the mixing endmembers, whereas rims may record the isotopic ratio of the post-mixing hybrid magma (Davidson et al., 2007). The isotopic character of the leachate, therefore, could be a complicated interplay of (1) the nature of open-system processes, leading to within-rock isotopic disequilibrium and (2) which mineral phases were preferentially dissolved.

The Sedlečko lahar (V3 lithofacies) is more radiogenic ($^{87}Sr/^{86}Sr$ composition *ca* 0.7048; Table 3) than any of the analysed lava (Rapprich & Holub, 2008). Such a shift seems to be too pronounced even after long-term selective leaching of the less radiogenic Sr fraction. Moreover, it is expected that the lahar represents a range of basaltic rocks, not only those with more radiogenic $^{87}Sr/^{86}Sr$. Present day $^{87}Sr/^{86}Sr$ composition may thus also be influenced by long-term groundwater circulations contributing small amounts of highly radiogenic Sr from country-rock granites (Dolejš et al., 2016).

20554877, 2023, 4, Downloaded from https://onlinelibrary.wiley.com/doi/10.1002/dep2.240 by Cochrane Hungary, Wiley Online Library on [05/12/2023]. See the Terms and Conditions (https://onlinelibrary.wiley.com/terms-and-conditions) on Wiley Online Library for rules of use; OA articles are governed by the applicable Creative Commons License

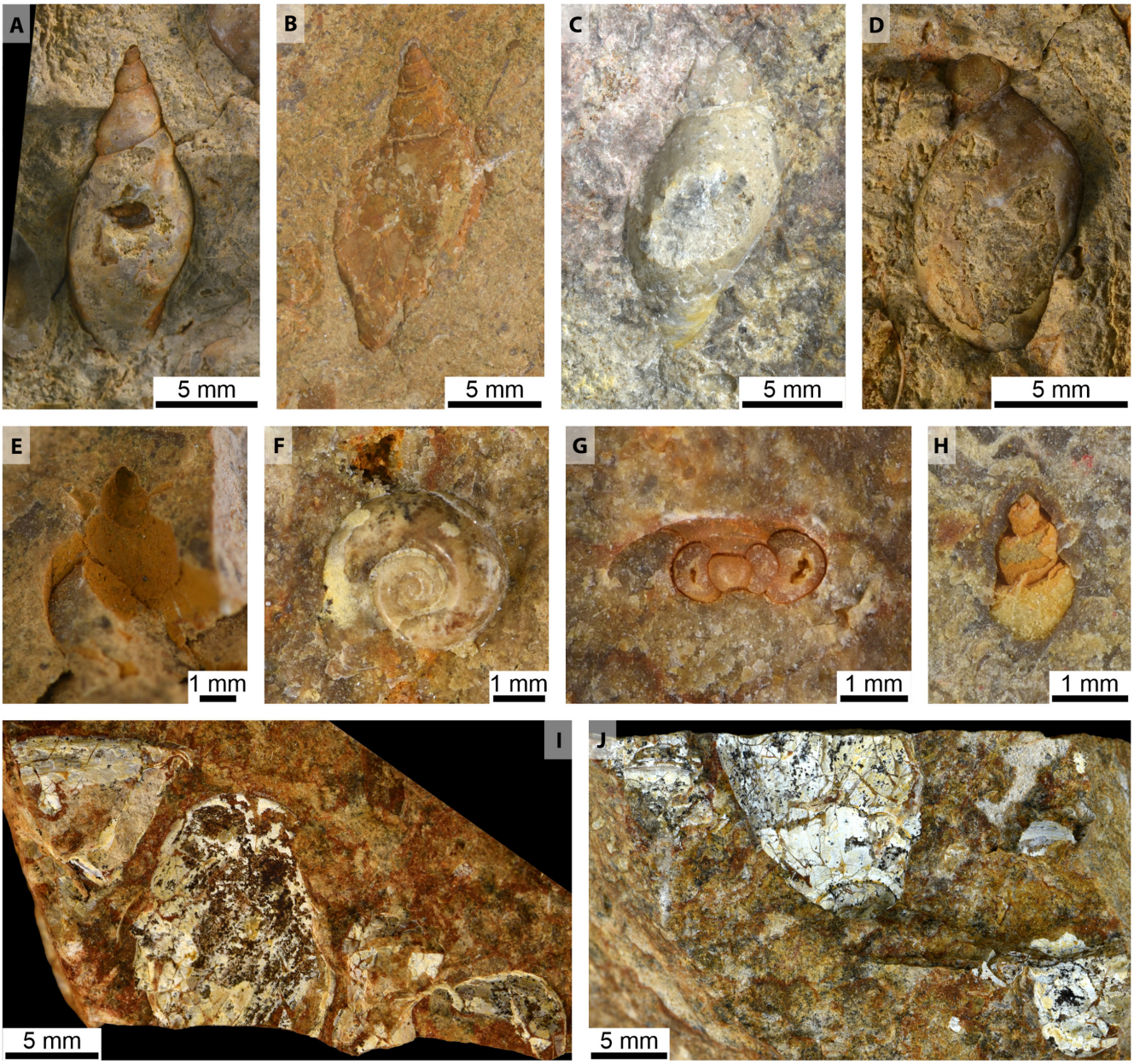

FIGURE 10 Fossils collected from limestones at Sedlečko excavation. (A) *Stagnicola* sp.—preserved core/filling of dissolved shell uncovered by natural weathering. (B) *Stagnicola* sp.—flattened shell-core on the crash-surface. (C, D) *Radix* sp.—preserved core/filling of dissolved shell uncovered by natural weathering. (E)?*Radix* sp. imprint of the shell. (F) *Planorbis* sp.—preserved core/filling of dissolved shell on the crash-surface. (G) *Planorbis* sp.—cross section of core of partly dissolved incomplete shell. (H) Part of core of dissolved shell of undetermined gastropod on the crash-surface. (I, J) Parts of flattened and shattered gastropod shells.

Focussing on the Sr isotopic composition, it can be observed that limestones from the Dubina and Sedlečko brecciated travertine have an even less radiogenic $^{87}Sr/^{86}Sr$ composition (0.7038–0.7041) than any of the lavas analysed by Rapprich and Holub (2008; Figure 9). That paper describes late Rupelian to Chattian (post 28 Ma) lavas, but Holub et al. (2010) analysed slightly older (29–30 Ma) intrusive alkaline rocks from the DHVC, suggesting compositionally similar lavas with lower $^{87}Sr/^{86}Sr$ values (as low as 0.7036; Figure 9) could have erupted during an earlier stage in the evolution of the DHVC. Weathering of these early Oligocene (Rupelian) low $^{87}Sr/^{86}Sr$ lavas seems to be an adequate candidate for the source of CaO precipitated in the Dubina limestones and Sedlečko brecciated travertine. The shift in $^{87}Sr/^{86}Sr$ towards more radiogenic values for the Sedlečko limestones might be explained by inclusion of a greater proportion of late Oligocene (higher $^{87}Sr/^{86}Sr$) lavas into the source lahars. Such a scenario is contradicted by the low $^{87}Sr/^{86}Sr$ values for Sedlečko brecciated travertine, which should (according to its position) be a product of the same source. More likely,

20554877, 2023, 4, Downloaded from https://onlinelibrary.wiley.com/doi/10.1002/dep2.240 by Cochrane Hungary, Wiley Online Library on [05/12/2023]. See the Terms and Conditions (https://onlinelibrary.wiley.com/terms-and-conditions) on Wiley Online Library for rules of use; OA articles are governed by the applicable Creative Commons License

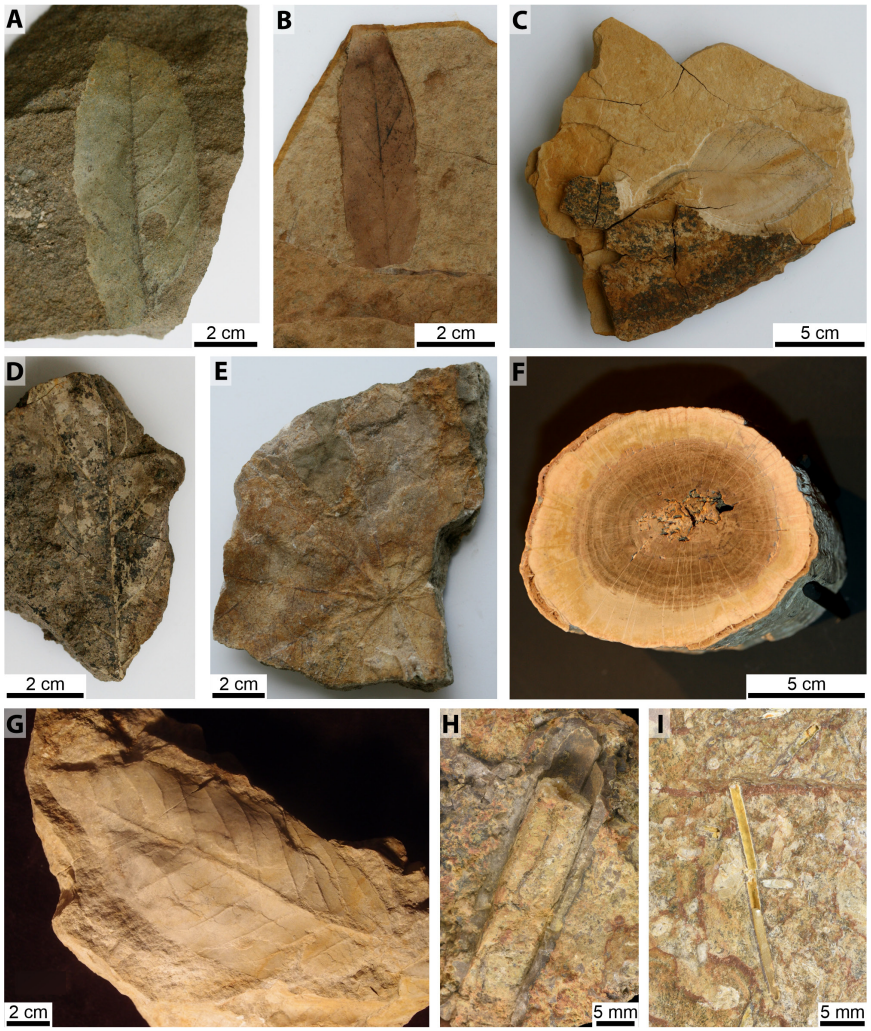

FIGURE 11 Plant remnants. (A, B) *Platanus neptuni*, Dubina (A—lahar, B—limestone). (C) *Populus* sp., Dubina limestone. (D) *Eotrigonobalanus furcinervis*, Sedlečko lahar. (E) *Craigia bronnii*, Sedlečko limestone. (F, G) *Alnus* sp., Sedlečko limestone (F—wood, G—leaf). (H, I) Completely recrystallised branches, roots or reed rhizomes, Sedlečko limestone.

TABLE 4 Results of K-Ar geochronological analyses.

Sample	ATOMKI lab-code	Fraction (mm)	*K* (%)	^{40}Ar (×10^{-6} ccSTP/g)	^{40}Ar*/ ^{40}Ar$_{tot}$	Radiometric age (Ma)	Error (Ma)
DB02	9133	Bulk-rock 0.125–0.250	2.246	2.201	0.65	25.04	0.36
		Light groundmass 0.125–0.250	2.696	2.674	0.75	25.34	0.36
DR334	9138	Light groundmass 0.125–0.250	3.075	2.602	0.54	21.64	0.31

the brecciated travertine, as the outpouring site, carries the endmember Sr isotopic character of its source, whereas the lacustrine limestones were contaminated by radiogenic Sr washed to the lake from surrounding country-rock granite (Dolejš et al., 2016; see Figures 9 and 12).

Strikingly low ^{87}Sr/^{86}Sr values of verifiably sedimentary carbonate is then linked to the origin of Sr (and CaO by proxy) from weathering of basaltic lavas and does not represent any evidence of carbonatite activity. The origin of CaO from weathered basaltic rock is also supported by minor amounts of smectite (Figure 3C) and fine basaltic silt (Figure 7B) admixtures in the limestones.

5.4 | Mechanical interactions between lahars/debris avalanches and bio−/chemogenic sediments

Limestones in the Sedlečko quarry do not display signs of intense post-depositional deformation. A well-defined linear trend for all samples in the TiO_2 versus SiO_2 binary diagram suggests that most of the silica in the limestones is carried by fine volcanoclastic silt. The only exception deviating from this trend is the sample Sed-I_01 from Sedlečko quarry, which lacks TiO_2 (Figure 7B). This most likely resulting from secondary silicification, as no source

20554877, 2023, 4, Downloaded from https://onlinelibrary.wiley.com/doi/10.1002/dep2.240 by Cochrane Hungary, Wiley Online Library on [05/12/2023]. See the Terms and Conditions (https://onlinelibrary.wiley.com/terms-and-conditions) on Wiley Online Library for rules of use; OA articles are governed by the applicable Creative Commons License

of detrital quartz was available in the area of the shield volcano. Sedimentary rocks in the Dubina section are then affected by more complex post-depositional recrystallisation and deformation.

Besides weaker silicification, represented by smaller amounts of opal in F2a facies impregnating the porous structure produced by partial leaching of the limestone, the finely laminated sediments display intense deformation. Discrete folding at a millimetre-scale is clearly visible in both limestones (Figure 3D,E,F) and diatomites (Figure 4D,E). Additionally, the originally whitish diatomites in many places transition to dark massive rock (Figure 4B,E), suggesting compression and recrystallisation of initially highly porous (and low specific weight) material. All of these deformation features are restricted to close relationships with jig-saw fractured block-containing debrite (V2) facies (Figure 2A,D). Well-developed jig-saw fit fractures within the blocks and boulders (or even mega-blocks), partly filled with matrix, are indicative of debris avalanche deposits (Alloway et al., 2005; Bustos et al., 2022). The DHVC volcano extends *ca* 25 km across (studied sites are *ca* 11 km from the central part of the volcano), originally rising at least 600 m (more likely 800–900 m) above its basement.

Due to significant erosion since the Late Oligocene, it is challenging to reconstruct the volume of individual debris avalanches created during volcano evolution. Deformation, compression and recrystallisation observed in the Dubina sediments is closely and exclusively associated with the exposure of the debris avalanche deposit (V2 lithofacies). In addition, very detailed deformation suggests rapid and short events that most likely reflect indentation of the debris avalanche. Discrete (millimetre-scale) folding represented by stylolite-type structures in both laminated limestones and diatomites suggest at least partial lithification of the deposits prior to deformation, as liquification and roiling would appear in the case of non-lithified sediments (Marco & Agnon, 1995). The discrete and spatially limited character of the deformation suggest rapid and instant event, rather than a dragging process (creeping, spreading, or similar), which would produce more dispersed deformation with long-wave and low-amplitude folds (Katsman, 2013; Pietruszczak et al., 2002). Close space relationships between the deformed domains of the laminated sediments and the debris avalanche deposits suggest a genetic relationship between both features.

Deformation and bulldozing effects of sedimentary substrata and sediments at the volcano periphery indented by debris avalanche are known from the 10 ka collapse of the Jocotitlán volcano in Central México (Dufresne et al., 2010). Shock-metamorphosis associated with the impact of a debris avalanche onto the volcano basement in the French Massif Central created temperatures of around 800°C, possibly up

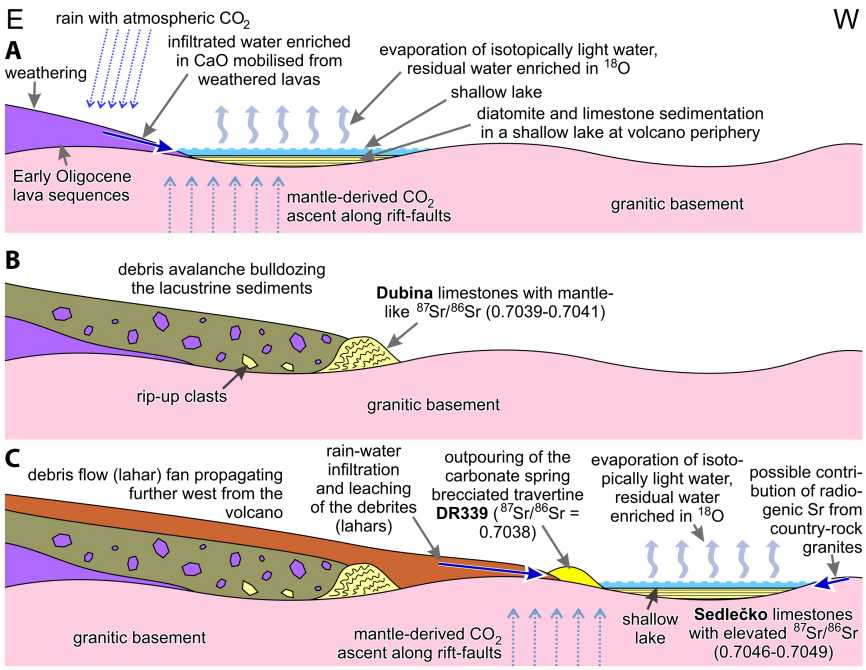

FIGURE 12 Schematic model of carbonate sedimentation and deformation at the western periphery of the Doupovské Hory volcano. (A) Lacustrine carbonate deposition in a shallow Late Oligocene palaeolake (Dubina) with reactants supplied from weathering of early DHVC lavas. (B) Deposition of debris avalanche leading to deformation of the Dubina lacustrine deposits. (C) Shift of the lacustrine sedimentation further west of the volcano, with mantle-derived CO_2-rich efflorescence producing a travertine mound (Sedlečko excavation). More radiogenic $^{87}Sr/^{86}Sr$ signature in the lacustrine limestones (Sedlečko quarry) suggests possible contribution from country-rock granites to chemistry of limestone precipitated in the Sedlečko palaeolake.

20554877, 2023, 4, Downloaded from https://onlinelibrary.wiley.com/doi/10.1002/dep2.240 by Cochrane Hungary, Wiley Online Library on [05/12/2023]. See the Terms and Conditions (https://onlinelibrary.wiley.com/terms-and-conditions) on Wiley Online Library for rules of use; OA articles are governed by the applicable Creative Commons License

to 1,500°C, and differential stress up to 10 GPa (Bernard & Van Wyk de Vries, 2017). Despite the debris avalanche in the studied area possibly being of smaller volume, transformation of kinetic energy into heat is well-documented in deep compaction and recrystallisation of the diatomites. Later debris flows, reaching as far as the Sedlečko area, did not have the potential to deform sedimentary rocks and served solely as source of CaO.

Carbonate springs and ponds formed at the front of agglomerate fans on the foothills of large volcanoes seems to be a potentially interesting sedimentary environment not well described in existing literature. The studies of volcano edifice failures mostly focus on calc-alkaline volcanoes at convergent plate boundaries (Capra et al., 2002; Jicha et al., 2015; Keigler et al., 2011; Roberti et al., 2017; Tost et al., 2014, 2015; Van Wyk de Vries et al., 2001); with different geochemistry and distinct weathering. Studies focussed on edifice failure processes at within-plate or continental-rift alkaline volcanoes are significantly scarcer (Delcamp et al., 2016; Kervyn et al., 2008), while reports on associated carbonate sedimentation are practically non-existent, although such deposits can be expected in these settings.

The entire development of the Dubina–Sedlečko volcano-sedimentary system, including its chemical evolution, is summarised in Figure 12. In the first stage, laminated lacustrine deposits at the volcano foothills were supplied from the weathering of basaltic lavas (Figure 12A). The laminated sedimentary sequence was deformed by indention caused by debris avalanches (Figure 12B). As a result, peripheral lacustrine sedimentation migrated further away from the volcano. A change in the local hydrological settings was documented to reflect deposition of Holocene avalanche debris on Parinacota, in central Andes (Jicha et al., 2015). As a consequence, the supply of CaO provided by the propagating distal debris flows (lahars) was also shifted further away from the volcano, but under increasing compositional influence exerted by country-rock granites (Figure 12C).

6 | CONCLUSIONS

- The studied localities at the foothills of the Doupovské Hory Mountains reveal a complex sedimentation history influenced in various ways by weathering and decay of the Oligocene alkali basaltic shield volcano.
- Sedimentation at the foothills of the Oligocene DHVC was strongly influenced by volcanic edifice failure processes. Epiclastic mass flows (debris flows and debris avalanches) supplied the peripheral lakes to a lesser extent with fine detritus, but mainly in calcium liberated from fragmented and weathered alkaline basaltic rocks. The shallow lake sediments became deformed by the bulldozer effect of moving debris avalanches.
- Fossil assemblages suggest significant seasonal water-level fluctuations, possibly reflecting the alternating rainy and dry-seasons of a generally humid, Central-European Oligocene climate. Seasonal drying out of the ponds likely resulted in ^{18}O enrichment.
- Limestones derived from weathered alkaline basalts are characterised by highly non-radiogenic Sr isotopic ratios ($^{87}Sr/^{86}Sr$ *ca* 0.704), suggesting a magmatic origin for these carbonates. It is possible to demonstrate on this spectacular example that Sr isotopes do not reveal the origin of carbonate rock, but rather, the source of Ca ions. Hence, carbonates with non-radiogenic Sr isotope systematics do not necessarily mean the presence of carbonatite.

ACKNOWLEDGEMENTS

This manuscript contributes to the Strategic Research Plan of the Czech Geological Survey (DKRVO/ČGS 2018-2022), projects 310950 and 310450. We are indebted to Bohuslava Čejková (ČGS) for analyses of C-O stable isotopes, to Zlatko Kvaček (†) for assistance with identification of palaeobotanic findings, and to John M. Hora and Greta Mackenzie for language checking. The manuscript benefited from constructive comments by Károly Németh and an anonymous reviewer.

DATA AVAILABILITY STATEMENT

All data used for this research are made available in the form of tables included in the manuscript.

ORCID

Vladislav Rapprich https://orcid.org/0000-0003-4349-2116
Pavel Čáp https://orcid.org/0000-0002-5329-4765
Yulia V. Erban Kochergina https://orcid.org/0000-0002-3938-8810
Jakub Sakala https://orcid.org/0000-0001-8922-0832
Daniel A. Petrash https://orcid.org/0000-0001-5039-0543

REFERENCES

Ackerman, L., Ulrych, J., Řanda, Z., Erban, V., Hegner, E., Magna, T., Balogh, K., Frána, J., Lang, M. & Novák, J.K. (2015) Geochemical characteristics and petrogenesis of phonolites and trachytic rocks from the České Středohoří Volcanic Complex, the Ohře Rift, Bohemian Massif. *Lithos*, 224, 256–271. https://doi.org/10.1016/j.lithos.2015.03.014

Agbulut, B., Tuncer, A., Tunoglu, C., Gümüs, B.A., Demir, S. & Özcan, E. (2020) Ostracod and gastropod fauna of the Alagöz Section (Central Anatolia): new fossil data for the Neogene lacustrine deposits of Ankara region. 2nd Palaeontological Virtual Congress, Valencia, İspanya, 1 - 15 Mayıs 2020, Book of Abstracts: Palaeontology in the virtual era, p. 149.

Alloway, B., McComb, P., Neall, V., Vucetich, C., Gibb, J., Sherburn, S. & Stirling, M. (2005) Stratigraphy, age, and correlation of voluminous debris-avalanche events from an ancestral Egmont Volcano:

20554877, 2023, 4, Downloaded from https://onlinelibrary.wiley.com/doi/10.1002/dep2.240 by Cochrane Hungary, Wiley Online Library on [05/12/2023]. See the Terms and Conditions (https://onlinelibrary.wiley.com/terms-and-conditions) on Wiley Online Library for rules of use; OA articles are governed by the applicable Creative Commons License

implications for coastal plain construction and regional hazard assessment. *Journal of the Royal Society of New Zealand*, 35, 229–267. https://doi.org/10.1080/03014223.2005.9517782

Bellon, H., Bůžek, Č., Gaudant, J., Kvaček, Z. & Walter, H. (1998) The Česke Středohoří magmatic complex in Northern Bohemia ^{40}K-^{40}Ar ages for volcanism and biostratigraphy of the Cenozoic freshwater formations. *Newsletters on Stratigraphy*, 36(2–3), 77–103. https://doi.org/10.1127/nos/36/1998/77

Bernard, K. & Van Wyk de Vries, B. (2017) Volcanic avalanche fault zone with pseudotachylite and gouge in French Massif Central. *Journal of Volcanology and Geothermal Research*, 347, 112–135. https://doi.org/10.1016/j.jvolgeores.2017.09.006

Boynton, W.V. (1984) Cosmochemistry of the rare earth elements: meteorite studies. In: Henderson, P. (Ed.) *Rare Earth Element Geochemistry. Developments in Geochemistry*. Amsterdam–New York: Elsevier, pp. 63–114.

Bustos, E., Capra, L., Arnosio, M. & Norini, G. (2022) Volcanic debris avalanche transport and emplacement at Chimpa volcano (Central Puna, Argentina): insights from morphology, grain-size and clast surficial textures. *Journal of Volcanology and Geothermal Research*, 432, 107671. https://doi.org/10.1016/j.jvolgeores.2022.107671

Buzek, F., Hanzlík, J., Hrubý, M. & Tryzna, P. (1991) Evaluation of the runoff components on the slope of an open-cast mine by means of environmental isotopes ^{18}O and T. *Journal of Hydrology*, 127, 23–36. https://doi.org/10.1016/0022-1694(91)90106-R

Cajz, V., Rapprich, V., Erban, V., Pécskay, Z. & Radoň, M. (2009) Late Miocene volcanic activity in the České středohoří Mountains (Ohře/Eger Graben, northern Bohemia). *Geologica Carpathica*, 60, 519–533. https://doi.org/10.2478/v10096-009-0038-8

Capra, L., Macıas, J.L., Scott, K.M., Abrams, M. & Garduño-Monroy, V.H. (2002) Debris avalanches and debris flows transformed from collapses in the Trans-Mexican Volcanic Belt, Mexico–behavior, and implications for hazard assessment. *Journal of Volcanology and Geothermal Research*, 113, 81–110. https://doi.org/10.1016/S0377-0273(01)00252-9

Chafetz, H.S. & Folk, R.L. (1984) Travertines: depositional morphology and the bacterially constructed constituents. *Journal of Sedimentary Petrology*, 54, 289–316. https://doi.org/10.1306/212F8404-2B24-11D7-8648000102C1865D

Cowardin, L.M., Carter, V., Golet, F.C. & LaRoe, E.T. (1979) Classification of wetlands and deepwater habitats of the United States. US Fish and Wildlife Service, FWS/OBS-79/31, 131 pp.

Davidson, J.P., Morgan, D.J., Charlier, B.L.A., Harlou, R. & Hora, J.M. (2007) Microsampling and isotopic analysis of igneous rocks: implications for the study of magmatic systems. *Annual Reviews in Earth and Planetary Sciences*, 35, 273–311. https://doi.org/10.1146/annurev.earth.35.031306.140211

Delcamp, A., Delvaux, D., Kwelwa, S., Macheyeki, A. & Kervyn, M. (2016) Sector collapse events at volcanoes in the North Tanzanian divergence zone and their implications for regional tectonics. *Geological Society of America Bulletin*, 128, 169–186. https://doi.org/10.1130/B31119.1

Dempírová, L., Šikl, J., Kašičková, R., Zoulková, V. & Kříbek, B. (2010) The evaluation of precision and relative error of the main components of silicate analyses in Central Laboratory of the Czech Geological Survey. *Zprávy o Geologických Výzkumech v roce*, 27, 326–330 (in Czech with English summary).

Dèzes, P., Schmid, S.M. & Ziegler, P.A. (2004) Evolution of the European Cenozoic Rift System: interaction of the Alpine and Pyrenean orogens with their foreland lithosphere. *Tectonophysics*, 389, 1–33. https://doi.org/10.1016/j.tecto.2004.06.011

Di Capua, A. & Groppelli, G. (2018) The riddle of volcaniclastic sedimentation in ancient deep-water basins: a discussion. *Sedimentary Geology*, 378, 52–60. https://doi.org/10.1016/j.sedgeo.2018.05.008

Dolejš, D., Bendl, J. & Štemprok, M. (2016) Rb-Sr isotopic composition of granites in the Western Krušné hory/Erzgebirge pluton, Central Europe: record of variations in source lithologies, mafic magma input and postmagmatic hydrothermal events. *Mineralogy and Petrology*, 110, 601–622. https://doi.org/10.1007/s00710-016-0434-6

Dufresne, A., Salinas, S. & Siebe, C. (2010) Substrate deformation associated with the Jocotitlán edifice collapse and debris avalanche deposit, Central México. *Journal of Volcanology and Geothermal Research*, 197, 133–148. https://doi.org/10.1016/j.jvolgeores.2010.02.019

Erban Kochergina, Y.V., Erban, V. & Hora, J.M. (2022) Sample preparation and chromatographic separation for Sr, Nd, and Pb isotope analysis in geological, environmental, and archaeological samples. *Journal of Geosciences*, 67, 273–285. doi:10.3190/jgeosci.357

Erban Kochergina, Y.V., Novák, M., Erban, V. & Štěpánová, M. (2021) ^{87}Sr/^{86}Sr isotope ratios in trees as an archaeological tracer: limitations of linking plant-biomass and bedrock Sr isotope signatures. *Journal of Archaeological Science*, 133, 105438. https://doi.org/10.1016/j.jas.2021.105438

Fejfar, O. & Kaiser, T.M. (2005) Insect bone-modification and paleoecology of Oligocene mammal-bearing sites in the Doupov Mountains, northwestern Bohemia. *Palaeontologia Electronica*, 8, 1–11.

Flügel, E. (2004) *Microfacies of carbonate rocks. Analysis, interpretation and application*. Berlin, Heidelberg, New York: Springer, pp. 1–976.

Fouke, B.W., Farmer, J.D., Des Marais, D.J., Pratt, L., Sturchio, N.C., Burns, P.C. & Discipulo, M.K. (2000) Depositional facies and aqueous–solid geochemistry of travertine-depositing hot springs (Angel Terrace, Mammoth Hot Springs, Yellowstone National Park, U.S.A.). *Journal of Sedimentary Research*, 70, 265–285. https://doi.org/10.1306/2DC40929-0E47-11D7-8643000102C1865D

Francis, P.W., Gardeweg, M., Ramirez, C.F. & Rothery, D.A. (1985) Catastrophic debris avalanche deposit of Socompa volcano, northern Chile. *Geology*, 13, 600–603.

Freytet, P. & Verrecchia, E.P. (2002) Lacustrine and palustrine carbonate petrography: an overview. *Journal of Paleolimnology*, 27, 221–237.

Garavelli, A., Laviano, R. & Vurro, F. (1997) Sublimate deposition from hydrothermal fluids at the Fossa crater-Vulcano, Italy. *European Journal of Mineralogy*, 9, 423–432.

Gillot, P.Y., Cornette, Y., Max, N. & Floris, B. (1992) Two reference materials, trachytes Mdo-G and Ish-G, for Argon dating (K-Ar and ^{40}Ar/^{39}Ar) of Pleistocene and Holocene rocks. *Geostandards Newsletter*, 16, 55–60. https://doi.org/10.1111/j.1751-908X.1992.tb00487.x

Glover, C. & Robertson, A.H. (2003) Origin of tufas (cool-water carbonate) and related terraces in the Antalya areas, SW Turkey. *Geological Journal*, 38, 1–30. https://doi.org/10.1002/gj.959

Glückselig, A.M. (1842) *Der Elbogner Kreis des Königreichs Böhmen*. Carlsbad und Elbogen: Gebrüder Franieck, p. 108.

Hays, P.D. & Grossman, E.L. (1991) Oxygen isotopes in meteoric calcite cements as indicators of continental palaeoclimate. *Geology*, 19, 441–444.

Hess, J.C. & Lippolt, H.J. (1994) Compilation of K-Ar measurements on HDB-1 standard biotite 1994 Status report. *Phanerozoic Time Scale*

20554877, 2023, 4, Downloaded from https://onlinelibrary.wiley.com/doi/10.1002/dep2.240 by Cochrane Hungary, Wiley Online Library on [05/12/2023]. See the Terms and Conditions (https://onlinelibrary.wiley.com/terms-and-conditions) on Wiley Online Library for rules of use; OA articles are governed by the applicable Creative Commons License

Bulletin of Liaison and Information of the IUGS Subcommission on Geochronology, 12, 19–21.

Holub, F.V., Rapprich, V., Erban, V., Pécskay, Z., Mlčoch, B. & Míková, J. (2010) Petrology and geochemistry of the Tertiary alkaline intrusive rocks at Doupov, Doupovské Hory Volcanic Complex (NW Bohemian Massif). *Journal of Geosciences*, 55, 251–278. https://doi.org/10.3190/jgeosci.074

Hroch, T., Rajchl, M., Kraft, P. & Rapprich, V. (2012) Sedimentary record of subaerial volcanic activity in the basal Ordovician shoal-marine deposits: the Třenice Formation of the Prague Basin, Bohemian Massif, Czech Republic. *Bulletin of Geosciences*, 87, 359–372. https://doi.org/10.3140/bull.geosci.1303

Janoušek, V., Farrow, C.M. & Erban, V. (2006) Interpretation of whole-rock geochemical data in igneous geochemist try: introducing Geochemical Data Toolkit (GCDkit). *Journal of Petrology*, 47, 1255–1259. https://doi.org/10.1093/petrology/egl013

Jicha, B.R., Laabs, B.J., Hora, J.M., Singer, B.S. & Caffee, M.W. (2015) Early Holocene collapse of Volcán Parinacota, central Andes, Chile: volcanological and paleohydrological consequences. *GSA Bulletin*, 127(11–12), 1681–1688. https://doi.org/10.1130/B31247.1

Kataoka, K.S., Manville, V., Nakajo, T. & Urabe, A. (2009) Impacts of explosive volcanism on distal alluvial sedimentation: examples from the Pliocene-Holocene volcaniclastic successions of Japan. *Sedimentary Geology*, 220, 306–317. https://doi.org/10.1016/j.sedgeo.2009.04.016

Katsman, R. (2013) Sediment undulations induced by free gas in muddy marine sediments: a modeling approach. *Geophysical Research Letters*, 40(13), 3379–3383. https://doi.org/10.1002/grl.50629

Keigler, R., Thouret, J.C., Hodgson, K.A., Neall, V.E., Lecointre, J.A., Procter, J.N. & Cronin, S.J. (2011) The Whangaehu Formation: debris-avalanche and lahar deposits from ancestral Ruapehu volcano, New Zealand. *Geomorphology*, 133(1–2), 57–79. https://doi.org/10.1016/j.geomorph.2011.06.019

Kerney, M.P., Cameron, R.A.D. & Jungbluth, J.H. (1983) *Die Landschnecken Nord- und Mitteleuropas*. Hamburg, Berlin: Paul Parey Verlag, p. 384.

Kervyn, M., Ernst, G.G.J., Klaudius, J., Keller, J., Mbede, E. & Jacobs, P. (2008) Remote sensing study of sector collapses and debris avalanche deposits at Oldoinyo Lengai and Kerimasi volcanoes, Tanzania. *International Journal of Remote Sensing*, 29, 6565–6595. https://doi.org/10.1080/01431160802168137

Kochergina, Y.V., Udatný, M., Penížek, V. & Mihaljevič, M. (2017) Mobility of Pb, Zn, Cu and As in disturbed forest soils affected by acid rain. *Environmental Monitoring and Assessment*, 189, 1–12. https://doi.org/10.1007/s10661-017-6306-7

Koutecký, V., Teodoridis, V., Čáp, P., Mantzouka, D. & Sakala, J. (2019) Fossil wood from the Doupovské hory and České středohoří volcanic complexes: latest overview and new angiosperms from the locality Dvérce. *Neues Jahrbuch für Geologie und Paläontologie, Abhandlungen*, 293(3), 283–306. https://doi.org/10.1127/njgpa/2019/0842

Kühn, M., Karstens, J., Berndt, C. & Watt, S.F. (2021) Seismic reconstruction of seafloor sediment deformation during volcanic debris avalanche emplacement offshore Sakar, Papua New Guinea. *Marine Geology*, 439, 106563. https://doi.org/10.1016/j.margeo.2021.106563

Kvaček, Z. (2002) Late Eocene landscape, ecosystems and climate in northern Bohemia with particular reference to the locality of Kučlín near Bílina. *Bulletin of the Czech Geological Survey*, 77(3), 217–236.

Kvaček, Z. & Walther, H. (1995) The Oligocene volcanic flora of Suletice-Berand near Usti nad Labem, North Bohemia—a review. *Acta Musei Nationalis Pragae, Series S, Historia Nataturalis*, 50(1–4), 25–54.

Kvaček, Z. & Walther, H. (2001) The Oligocene of Central Europe and the development of forest vegetation in space and time based on megafossils. *Palaeontographica Abteilung B*, 259(1–6), 125–148. https://doi.org/10.1127/palb/259/2001/125

Kvaček, Z. & Walther, H. (2003) Reconstruction of vegetation and landscape development during volcanic activity in the České Středohoří Mountains. *GeoLines*, 15, 60–64.

Li, S., Xing, Y., Valdes, P.J., Huang, Y., Su, T., Farnsworth, A., Lunt, D.J., Tang, H., Kennedy, A.Z. & Zhou, Z. (2018) Oligocene climate signals and forcings in Eurasia revealed by plant macrofossil and modelling results. *Gondwana Research*, 61, 115–127. https://doi.org/10.1016/j.gr.2018.04.015

Ložek, V. (1964) Die Quartärmollusken der Tschechoslowakei. *Rozpravy Ústredního ústavu geologického*, 31, 1–374.

Mach, K. & Dvořák, Z. (2011) Geology of the site Kučlín, Trupelník Hill near Bílina in North Bohemia. *Acta Musei Nationalis Pragae (B)*, 67, 77–82.

Mach, K., Žák, K., Teodoridis, V. & Kvaček, Z. (2017) Consequences of lower Miocene CO_2 degassing on geological and paleoenvironmental settings of the Ahníkov/Merkur Mine paleontological locality (Most Basin, Czech Republic). *Neues Jahrbuch für Geologie und Paläontologie-Abhandlungen*, 285(3), 235–266. https://doi.org/10.1127/njgpa/2017/0680

Malz, H. & Moayedpour, E. (1973) Miozäne Süßwasser-Ostracoden aus der Rhön. *Senckenbergiana Lethaea*, 54(2/4), 281–309 5 Abb., 5 Taf., Frankfurt am Main.

Manville, V., Németh, K. & Kano, K. (2009) Source to sink: a review of three decades of progress in the understanding of volcaniclastic processes, deposits, and hazards. *Sedimentary Geology*, 220, 136–161. https://doi.org/10.1016/j.sedgeo.2009.04.022

Marco, S. & Agnon, A. (1995) Prehistoric earthquake deformations near Masada, Dead Sea graben. *Geology*, 23(8), 695–698.

Martí, J., Groppelli, G. & Brum da Silveira, A. (2018) Volcanic stratigraphy: a review. *Journal of Volcanology and Geothermal Research*, 357, 68–91. https://doi.org/10.1016/j.jvolgeores.2018.04.006

Martin-Bello, L., Arenas, C. & Jones, B. (2019) Lacustrine stromatolites: useful structures for environmental interpretation. An example from the Miocene Ebro Basin. *Sedimentology*, 66, 2098–2133. https://doi.org/10.1111/sed.12577

Matsumo, A. & Kobayashi, T. (1995) K/Ar age determination of late Quaternary volcanic rocks using the "mass fractionation correction procedure": application to the Younger Ontake Volcano, Central Japan. *Chemical Geology*, 125, 123–135. https://doi.org/10.1016/0009-2541(95)00062-Q

McCrea, J.M. (1950) On the isotope chemistry of carbonates and a paleotemperature scale. *The Journal of Chemical Physics*, 18, 849–857.

Mlčoch, B. & Konopásek, J. (2010) Pre-Late Carboniferous geology along the contact of the Saxothuringian and Teplá-Barrandian zones in the area covered by younger sediments and volcanics (western Bohemian Massif, Czech Republic). *Journal of Geosciences*, 55, 81–94. https://doi.org/10.3190/jgeosci.068

Moser, M., Niederhöfer, H.J. & Falkner, G. (2009) Continental molluscs of the fossil site Sandelzhausen (Miocene; Upper Freshwater Molasse from Bavaria) and their value for palaeoecological assessment. *Paläontologische Zeitschrift*, 83, 25–54. https://doi.org/10.1007/s12542-009-0013-9

Muir, M., Lock, D. & Von der Borch, C. (1980) The Coorong model for penecontemporaneous dolomite formation in the Middle

20554877, 2023, 4, Downloaded from https://onlinelibrary.wiley.com/doi/10.1002/dep2.240 by Cochrane Hungary, Wiley Online Library on [05/12/2023]. See the Terms and Conditions (https://onlinelibrary.wiley.com/terms-and-conditions) on Wiley Online Library for rules of use; OA articles are governed by the applicable Creative Commons License

Proterozoic McArthur Group, Northern Territory, Australia. In: Zenger, D.H., Dunham, J.B. & Ethington, R.L. (Eds.) *Concepts and models of dolomitization*. Houston: SEPM Special Publication.

Murray, J.B., Van Wyk De Vries, B., Pitty, A., Sargent, P. & Wooller, L. (2018) Gravitational sliding of the Mt. Etna massif along a sloping basement. *Bulletin of Volcanology*, 80, 1–11. https://doi.org/10.1007/s00445-018-1209-1

Nádaskay, R., Kochergina, Y.V., Čech, S., Švábenická, L., Valečka, J., Erban, V., Halodová, P. & Čejková, B. (2019) Integrated stratigraphy of an offshore succession influenced by intense siliciclastic supply: implications for Coniacian tectono-sedimentary evolution of the West Sudetic area (NW Bohemian Cretaceous Basin, Czech Republic). *Cretaceous Research*, 102, 127–159. https://doi.org/10.1016/j.cretres.2019.06.005

Novo, T.A., Pedrosa-Soares, A., Vieira, V.S., Dussin, I. & da Silva, L.C. (2018) The Rio Doce Group revisited: an Ediacaran arc-related volcano-sedimentary basin, Araçuaí orogen (SE Brazil). *Journal of South American Earth Sciences*, 85, 345–361. https://doi.org/10.1016/j.jsames.2018.05.013

Ollier, G., Cochonat, P., Lenat, J.F. & Labazuy, P. (1998) Deep-sea volcaniclastic sedimentary systems: an example from La Fournaise volcano, Reunion Island, Indian Ocean. *Sedimentology*, 45, 293–330.

O'Neil, J.R., Clayton, R.N. & Mayeda, T.K. (1968) Oxygen isotope fractionation in divalent metal carbonates. *The Journal of Chemical Physics*, 51, 5547–5558.

Pentecost, A. (2005) *Travertine*. Berlin Heidelberg: Springer-Verlag, p. 460.

Pentecost, A. & Viles, H. (1994) A review and reassessment of Travertine classification. *Geographie Physique et Quaternaire*, 48(3), 305–314.

Petrash, D.A., Bialik, O.M., Staudigel, P.T., Konhauser, K.O. & Budd, D.A. (2021) Biogeochemical reappraisal of the freshwater–seawater mixing-zone diagenetic model. *Sedimentology*, 68, 1797–1830. https://doi.org/10.1111/sed.12849

Pietruszczak, S., Lydzba, D. & Shao, J.F. (2002) Modelling of inherent anisotropy in sedimentary rocks. *International Journal of Solids and Structures*, 39(3), 637–648. https://doi.org/10.1016/S0020-7683(01)00110-X

Pokorný, V. (1986) Freshwater ostracodes from the Lower Miocene of Tuchořice (Bohemia, Czechoslovakia). *Acta Universitatis Carolinae*, 3, 281–315.

Quidelleur, X., Gillot, P.Y., Soler, V. & Lefèvre, J.C. (2001) K/Ar dating extended into the last millennium: application to the youngest effusive episode of the Teide volcano (Spain). *Geophysical Research Letters*, 28, 3067–3070. https://doi.org/10.1029/2000GL012821

Rajchl, M., Uličný, D., Grygar, R. & Mach, K. (2009) Evolution of basin architecture in an incipient continental rift: the Cenozoic Most Basin, Eger Graben (Central Europe). *Basin Research*, 21, 269–294. https://doi.org/10.1111/j.1365-2117.2008.00393.x

Rapprich, V., Cajz, V., Košťák, M., Pécskay, Z., Řídkošil, T., Raška, P. & Radoň, M. (2007) Reconstruction of eroded monogenic Strombolian cones of Miocene age: a case study on character of volcanic activity of the Jičín Volcanic Field (NE Bohemia) and subsequent erosional rates estimation. *Journal of Geosciences*, 52, 169–180. https://doi.org/10.3190/jgeosci.011

Rapprich, V. & Dostalík, M. (2015) Debris avalanche deposits on periphery of the Doupovské hory Volcanic Complex exposed during construction of R6 highway near Bošov. *Geoscience Research Reports*, 48, 19–24.

Rapprich, V. & Holub, F.V. (2008) Geochemical variations within the Upper Oligocene-Lower Miocene lava succession of Úhošť Hill (NE margin of Doupovské hory Mts., Czech Republic). *Geological Quarterly*, 52, 253–268.

Reuss, A.E. (1854) *Kurze Übersicht der geol*. Praha: Verhältnisse Böhmens.

Reuss, A.E. (1863) *Geognostische Skizze der Umgebungen von Carlsbad, Marienbad und Francensbad*. Teplitz-Schönau: Adolf Becker, p. 111.

Reuss, A.E. & von Meyer, H. (1849) Die tertiären Süsswassergebilde des nördlichen Böhmens und ihre fossilen Thierreste. *Palaeontographica II*, 1, 1–42. Cassel.

Roberti, G., Friele, P., Van Wyk de Vries, B., Ward, B., Clague, J.J., Perotti, L. & Giardino, M. (2017) Rheological evolution of the Mount Meager 2010 debris avalanche, southwestern British Columbia. *Geosphere*, 13(2), 1–22. https://doi.org/10.1130/GES01389.1

Rojík, P. (2013) Geological substrates and heaping process of coal mining operations in the Sokolov Basin, Czech Republic. In: Frouz, J. (Ed.) *Soil biota and ecosystem development in post mining sites*. Boca Raton, Florida: CRC Press, pp. 1–18.

Sakala, J., Rapprich, V. & Pécskay, Z. (2010) Fossil angiosperm wood and its host deposits from the periphery of a dominantly effusive ancient volcano (Doupovské hory Volcanic Complex, Oligocene-Lower Miocene, Czech Republic): systematics, volcanology, geochronology and taphonomy. *Bulletin of Geosciences*, 85, 617–629. https://doi.org/10.3140/bull.geosci.1196

Sanders, J.E. & Friedman, G.M. (1967) Origin and occurrence of limestones. In: Chilinger, G.V., Bissell, H.J. & Fairbridge, R.W. (Eds.) *Carbonate rocks*, Developments in Sedimentology, vol., Vol. 9a. Amsterdam: Elsevier, p. 322.

Schaller, J. (1785) *Topographie des Königreichs Böhmen: Th. Ellbogner Kreis (Vol. 2)*. Prag: W. Piskaczek.

Steiger, R.H. & Jäger, E. (1977) Subcommission on geochronology: convention on the use of decay constants in geo- and cosmochronology. *Earth and Planetary Science Letters*, 36, 359–362.

Teodoridis, V. & Kvaček, Z. (2015) Palaeoenvironmental evaluation of Cainozoic plant assemblages from the Bohemian Massif (Czech Republic) and adjacent Germany. *Bulletin of Geosciences*, 90, 695–720. https://doi.org/10.3140/bull.geosci.1553

Tibaldi, A. & Lagmay, A.M.F. (2006) Interaction between volcanoes and their basement. *Journal of Volcanology and Geothermal Research*, 158, 1–5. https://doi.org/10.1016/j.jvolgeores.2006.04.011

Tost, M., Cronin, S.J. & Procter, J.N. (2014) Transport and emplacement mechanisms of channelised long-runout debris avalanches, Ruapehu volcano, New Zealand. *Bulletin of Volcanology*, 76, 1–14. https://doi.org/10.1007/s00445-014-0881-z

Tost, M., Cronin, S.J., Procter, J.N., Smith, I.E.M., Neall, V.E. & Price, R.C. (2015) Impacts of catastrophic volcanic collapse on the erosion and morphology of a distal fluvial landscape: Hautapu River, Mount Ruapehu, New Zealand. *Geological Society of America Bulletin*, 127(1–2), 266–280. https://doi.org/10.1130/B31010.1

Ulrych, J., Dostal, J., Adamovič, J., Jelínek, E., Špaček, P., Hegner, E. & Balogh, K. (2011) Recurrent Cenozoic volcanic activity in the Bohemian massif (Czech Republic). *Lithos*, 123, 133–144. https://doi.org/10.1016/j.lithos.2010.12.008

Van Wyk de Vries, B.W., Self, S., Francis, P.W. & Keszthelyi, L. (2001) A gravitational spreading origin for the Socompa debris avalanche. *Journal of Volcanology and Geothermal Research*, 105, 225–247. https://doi.org/10.1016/S0377-0273(00)00252-3

Vasileiadou, K., Böhme, M., Neubauer, T.A., Georgalis, G.L., Syrides, G.E., Papadopoulou, L. & Zouros, N. (2017) Early Miocene gastropod and ectothermic vertebrate remains from the Lesvos Petrified

20554877, 2023, 4, Downloaded from https://onlinelibrary.wiley.com/doi/10.1002/dep2.240 by Cochrane Hungary, Wiley Online Library on [05/12/2023]. See the Terms and Conditions (https://onlinelibrary.wiley.com/terms-and-conditions) on Wiley Online Library for rules of use; OA articles are governed by the applicable Creative Commons License

Forest (Greece). *Paläontologische Zeitschrift*, 91, 541–564. https://doi.org/10.1007/s12542-017-0352-x

Villa, I.M., De Bièvre, P., Holden, N.E. & Renne, P.R. (2015) IUPAC-IUGS recommendation on the half-life of ^{87}Rb. *Geochimica et Cosmochimica Acta*, 164, 382–385. https://doi.org/10.1016/j.gca.2015.05.025

Villa, I.M., Holden, N.E., Possolo, A., Ickert, R.B., Hibbert, D.B. & Renne, P.R. (2020) IUPAC-IUGS recommendation on the half-lives of ^{147}Sm and ^{146}Sm. *Geochimica et Cosmochimica Acta*, 285, 70–77. https://doi.org/10.1016/j.gca.2020.06.022

Vylita, T. & Žák, K. (2009) Travertine deposits of the Karlovy Vary thermal water system. *Environmental Geology*, 58, 1639–1644. https://doi.org/10.1007/s00254-008-1484-9

Watt, S.F.L., Talling, P.J., Vardy, M.E., Masson, D.G., Henstock, T.J., Hühnerbach, V., Minshull, T.A., Urlaub, M., Lebas, E., Le Friant, A., Berndt, C., Crutchley, G.J. & Karstens, J. (2012) Widespread and progressive seafloor-sediment failure following volcanic debris avalanche emplacement: landslide dynamics and timing offshore Montserrat, Lesser Antilles. *Marine Geology*, 323, 69–94. https://doi.org/10.1016/j.epsl.2011.11.032

White, J.D.L. & Riggs, N.R. (2009) *Volcaniclastic sedimentation in lacustrine settings*. New York: John Wiley & Sons, pp. 1–309.

Witt, V. (2001) Lower Miocene freshwater ostracods from the Merkur-North open-cast mine (Most Basin, northern Bohemia, Czech Republic). *Bulletin Czech Geological Survey*, 76, 227–234.

Witt, V. (2002) Zur Süsswasserostracodenfauna der oligo-miozänen Vorlandmolasse Süddeutschlands. Mitteilungen der Bayerischen Staatssammlung für Paläontologie und Histor. *Geologie*, 42, 34–49.

Wright, V.P. (1990) Lacustrine carbonates. In: Tucker, M. & Wright, V.P. (Eds.) *Carbonate sedimentology*. Oxford: Blackwell, pp. 164–189.

Zerlik, O., Pleier, J. & Keil, E. (1974) *Die Karlsbader Landschaft*. Eichstätt: Das Buch der Heimat. Brönner & Daentler KG, p. 976.

How to cite this article: Rapprich, V., Čáp, P., Erban Kochergina, Y.V., Kadlecová, E., Benkó, Z., Sakala, J. et al. (2023) Interactions between distal epiclastic and bio-chemogenic sedimentation at the foothills of a mafic alkaline volcano: The case of the Oligocene Doupovské Hory Volcanic Complex (Czech Republic). *The Depositional Record*, 9, 871–894. Available from: https://doi.org/10.1002/dep2.240

20554877, 2023, 4, Downloaded from https://onlinelibrary.wiley.com/doi/10.1002/dep2.240 by Cochrane Hungary, Wiley Online Library on [05/12/2023]. See the Terms and Conditions (https://onlinelibrary.wiley.com/terms-and-conditions) on Wiley Online Library for rules of use; OA articles are governed by the applicable Creative Commons License